bioRxiv preprint doi: https://doi.org/10.1101/2023.03.14.532493; this version posted March 15, 2023. The copyright holder for this preprint (which was not certified by peer review) is the author/funder, who has granted bioRxiv a license to display the preprint in perpetuity. It is made available under aCC-BY-NC-ND 4.0 International license.

1
2
3
4 # Inhibitory input directs astrocyte morphogenesis through glial
5 # $GABA_BR$
6
7
8 Yi-Ting Cheng [1,2], Estefania Luna-Figueroa[1,3], Junsung Woo[1,3], Hsiao-Chi Chen[1,5], Zhung-Fu
9 Lee[1,4], Akdes Serin Harmanci[1,3], and Benjamin Deneen[1-6]*
10
11
12
13 [1] Center for Cancer Neuroscience, Baylor College of Medicine, Houston TX 77030

14 [2] Program in Developmental Biology, Baylor College of Medicine, Houston TX 77030

15 [3] Center for Cell and Gene Therapy, Baylor College of Medicine, Houston TX 77030

16 [4] Development, Disease, Models, and Therapeutics Graduate Program, Baylor College

17 of Medicine, Houston, TX 77030

18 [5] Cancer Cell Biology Graduate Program, Baylor College of Medicine, Houston TX

19 77030

20 [6] Department of Neurosurgery, Baylor College of Medicine, Houston TX 77030

21
22
23
24
25 *Correspondence: deneen@bcm.edu
26
27
28
29
30
31
32
33
34
35
36
37
38

bioRxiv preprint doi: https://doi.org/10.1101/2023.03.14.532493; this version posted March 15, 2023. The copyright holder for this preprint (which was not certified by peer review) is the author/funder, who has granted bioRxiv a license to display the preprint in perpetuity. It is made available under aCC-BY-NC-ND 4.0 International license.

39
40
41 **Abstract**

42 Communication between neurons and glia plays an important role in establishing and
43 maintaining higher order brain function. Astrocytes are endowed with complex
44 morphologies which places their peripheral processes in close proximity to neuronal
45 synapses and directly contributes to their regulation of brain circuits. Recent studies
46 have shown that excitatory neuronal activity promotes oligodendrocyte differentiation;
47 whether inhibitory neurotransmission regulates astrocyte morphogenesis during
48 development is unknown. Here we show that inhibitory neuron activity is necessary and
49 sufficient for astrocyte morphogenesis. We found that input from inhibitory neurons
50 functions through astrocytic $GABA_BR$ and that its deletion in astrocytes results in a loss
51 of morphological complexity across a host of brain regions and disruption of circuit
52 function. Expression of $GABA_BR$ in developing astrocytes is regulated in a region-
53 specific manner by SOX9 or NFIA and deletion of these transcription factors results in
54 region-specific defects in astrocyte morphogenesis, which is conferred by interactions
55 with transcription factors exhibiting region-restricted patterns of expression. Together
56 our studies identify input from inhibitory neurons and astrocytic $GABA_BR$ as universal
57 regulators of morphogenesis, while further revealing a combinatorial code of region-
58 specific transcriptional dependencies for astrocyte development that is intertwined with
59 activity-dependent processes.

60

61

62

bioRxiv preprint doi: https://doi.org/10.1101/2023.03.14.532493; this version posted March 15, 2023. The copyright holder for this preprint (which was not certified by peer review) is the author/funder, who has granted bioRxiv a license to display the preprint in perpetuity. It is made available under aCC-BY-NC-ND 4.0 International license.

63

64 Astrocytes are endowed with an extraordinarily complex morphology highlighted by
65 peripheral processes that are in close proximity to neuronal synapses[1–3]. These
66 elaborate processes contribute to a host of synaptic functions, ultimately impacting
67 circuit-level activities as it is estimated that a single astrocyte can interface with up to
68 100,000 synapses[4]. The acquisition of complex astrocyte morphologies during
69 development is essential for the execution of these roles and has wide-ranging
70 implications for brain function and neurological disorders[5–8]. Communication between
71 astrocytes and neurons plays a critical role in astrocyte development[9,10]. Previously, it
72 was shown that structural interactions between developing astrocytes and neurons
73 contributes to the acquisition of their complexity[11]. Moreover, astrocytes from dark-
74 reared animals exhibit reduced territories and when coupled with evidence that
75 glutamatergic signaling influences astrocytic volume, raise the possibility that neuronal
76 activity itself may contribute to astrocyte morphogenesis[11–13]. Nevertheless, whether and
77 how neuronal activity contributes to astrocyte morphogenesis remains unclear.
78 Furthermore, what types of neurons and associated neurotransmitters provide activity-
79 dependent input to drive astrocyte complexity are also undefined.

80

81 **Inhibitory neurons promote astrocyte morphogenesis**

82 The acquisition of complex astrocyte morphologies in the developing cortex occurs
83 during the P1-P28 developmental window, where the Aldh1l1-GFP reporter exhibits
84 selective expression in developing astrocytes[14,15]. To determine whether activation of
85 inhibitory neurons promotes astrocyte morphogenesis, we performed intraventricular

bioRxiv preprint doi: https://doi.org/10.1101/2023.03.14.532493; this version posted March 15, 2023. The copyright holder for this preprint (which was not certified by peer review) is the author/funder, who has granted bioRxiv a license to display the preprint in perpetuity. It is made available under aCC-BY-NC-ND 4.0 International license.

86 injection of AAV2/9 hDlx-hM3Dq-dTomato into P1, Aldh1l1-GFP reporter mice. One
87 week post-injection, we treated mice with saline or 5 mg/Kg of clozapine N-oxide (CNO)
88 two times a day, for two weeks, harvesting at P21 (**Fig. 1a**)[16] and used slice recordings
89 to confirm increased activity in inhibitory neurons after CNO treatment (**Fig.1b**). We did
90 not observe any overt differences between the saline and CNO groups with respect to
91 astrocyte numbers (**Extended Data Fig. 1a-b**). To evaluate morphological complexity,
92 we imaged Aldh1l1-GFP expressing astrocytes from LII-LIII of the visual cortex, finding
93 that astrocytes from the CNO group exhibit an increase in their complexity, branch
94 points, and process length compared to controls (**Fig. 1c-e**). CNO treatment alone had
95 no impact on the morphological complexity of astrocytes (**Extended Data Fig. 1c**).
96 Using the same stimulation paradigm and harvesting at P60 did not reveal any
97 differences in astrocyte morphology, indicating that increases in complexity reflect
98 accelerated morphogenesis (**Extended Data Fig. 1f-g**). Next, we examined whether
99 interneuron activity is necessary for astrocyte morphogenesis by inhibiting their activity.
100 Similar to the above studies we performed intraventricular injection of AAV2/9 hDlx-
101 hM4Di-dTomato into P1, Aldh1l1-GFP reporter mice, treated with CNO, and harvested
102 at P21; slice recordings confirmed decreased activity in inhibitory neurons after CNO
103 treatment (**Fig.1b**). Analysis of astrocyte morphology in LII-LIII of the visual cortex,
104 revealed decreased complexity in the CNO group (**Fig.1g-i**). Together, these
105 observations indicate that input from inhibitory neurons contributes to astrocyte
106 morphogenesis in the developing cortex.

107 GABA is the predominant neurotransmitter released by inhibitory neurons;
108 therefore we interrogated expression of GABA-receptors in transcriptomic data from

bioRxiv preprint doi: https://doi.org/10.1101/2023.03.14.532493; this version posted March 15, 2023. The copyright holder for this preprint (which was not certified by peer review) is the author/funder, who has granted bioRxiv a license to display the preprint in perpetuity. It is made available under aCC-BY-NC-ND 4.0 International license.

109 developing Aldh1l1-GFP astrocytes. This analysis identified $GABA_B$ receptor (*Gabbr1*)
110 as upregulated in astrocytes during the P1-P14 interval in the cortex, hippocampus, and
111 olfactory bulb (OB) (**Extended Data Figs. 1e**). To determine whether *Gabbr1*
112 expression is associated with astrocyte morphogenesis, we performed RNAscope on
113 P21 cortical sections from CNO and saline groups, finding that its expression is
114 increased in Aldh1l1-GFP astrocytes when inhibitory neurons are activated (**Fig. 1f,j**).
115 These data implicate astrocytic *Gabbr1* as a prospective regulator of astrocyte
116 morphogenesis during development,
117

118 ***Gabbr1* regulates astrocyte morphogenesis**

119 These observations raise the question of whether astrocytic *Gabbr1* directly regulates
120 astrocyte morphogenesis during development. While the role of *Gabbr1* in neurons is
121 established, whether it contributes to astrocyte development is unknown[17,18]. To
122 examine the role of *Gabbr1* in astrocyte development in the brain, we generated the
123 *Gabbr1$^{fl/fl}$; Aldh1l1-CreER; Aldh1l1-GFP* (*Gabbr1-cKO*) mouse line[19], with the Aldh1l1-
124 CreER line specifically targeting astrocytes (**Extended Data Fig. 2e-h**). Treatment with
125 a single injection of tamoxifen at P1 led to efficient knockout across a host of brain
126 regions at P28 (**Fig. 2a-b**), having no effect on the number of Aldh1l1-GFP/$Sox9^+$
127 astrocytes at P28 in the cortex, OB, hippocampus (CA1), and brainstem (**Extended**
128 **Data Fig. 3f-g**). Next, we assessed morphological complexity of astrocytes from the
129 *Gabbr1-cKO* at P28, focusing on layer II-III (LII-LIII) of the visual cortex, external
130 plexiform layer (EPL) OB, CA1 in the hippocampus, the internal granule layer (IGL) in
131 the cerebellum, and the medulla in the brainstem. We found that knockout of *Gabbr1*

bioRxiv preprint doi: https://doi.org/10.1101/2023.03.14.532493; this version posted March 15, 2023. The copyright holder for this preprint (which was not certified by peer review) is the author/funder, who has granted bioRxiv a license to display the preprint in perpetuity. It is made available under aCC-BY-NC-ND 4.0 International license.

132 led to a reduction in astrocyte complexity, branch points, and process length in all the
133 examined brain regions (**Fig. 2c and Extended Data Fig. 3a-b**); these observations
134 were validated using sparse labeling and knockout of *Gabbr1* (**Extended Data Fig. 3c-**
135 **e**). Together, these data indicate that *Gabbr1* is a universal regulator of astrocyte
136 morphogenesis. Next, we evaluated spontaneous $Ca2^{+}$ activity in the cortex of *Gabbr1-*
137 *cKO* and control mice at P28. Using a floxed-dependent GCaMP6 mouse line within our
138 *Gabbr1-cKO* line (**Fig. 2a**), followed by *ex vivo*, two-photon slice imaging at P28, we
139 found no changes in spontaneous $Ca2^{+}$ activity in cortical astrocytes from the *Gabbr1-*
140 *cKO* (**Fig. 2d; Extended Data Fig.6a**), suggesting physiological activities of astrocytes
141 are unaffected. Upon binding to GABA, astrocytic *Gabbr1* elicits $Ca2^{+}$ responses[20],
142 therefore we treated slices with baclofen, the $GABA_B$ receptor agonist, and found that
143 cortical astrocytes from the *Gabbr1-cKO* failed to generate a baclofen-induced $Ca2^{+}$
144 response (**Fig. 2e**). These data suggest that inhibitory input is disrupted in *Gabbr1-cKO*
145 astrocytes and in conjunction with our cellular analysis indicate that astrocytic *Gabbr1*
146 regulates morphogenesis.

147 Next, we examined whether inhibitory input functions through *Gabbr1* to regulate
148 astrocyte morphogenesis. To test this we injected the *Gabbr1-cKO* mouse line (and
149 control) at P1 with AAV2/9 hDlx-hM3Dq-dTomato and treated with CNO (**Fig.2f**).
150 Assessing astrocyte morphogenesis at P21 revealed that activation of inhibitory
151 neurons did not promote astrocyte morphogenesis in the *Gabbr1-cKO* (**Fig.2g-i**) and
152 that the extent of astrocyte complexity was similar to the *Gabbr1-cKO* (**Fig.2c v 2g-i**).
153 Collectively, these data indicate that inhibitory neurons drive astrocyte morphogenesis
154 through astrocytic *Gabbr1*.

bioRxiv preprint doi: https://doi.org/10.1101/2023.03.14.532493; this version posted March 15, 2023. The copyright holder for this preprint (which was not certified by peer review) is the author/funder, who has granted bioRxiv a license to display the preprint in perpetuity. It is made available under aCC-BY-NC-ND 4.0 International license.

155

156 **Astrocytic *Gabbr1* regulates cortical circuits**

157 The defects in astrocyte morphogenesis in the *Gabbr1-cKO* prompted us to perform
158 single-cell RNA Sequencing (scRNA-Seq) on *Gabbr1-cKO* and control cortices from
159 P28. Using Seurat analysis we identified the principle cell types in the brain and did not
160 observe any difference in their constituency (**Extended Data Fig. 4a-b**)[21]. Next, we
161 used the CellChat pipeline to map cell-cell interactions between astrocytes and
162 excitatory- and inhibitory- neurons from the scRNA-Seq datasets[22]. This analysis
163 revealed a decrease in the number of interactions between astrocytes and excitatory
164 neurons, coupled with an increase in the interaction between astrocytes and inhibitory
165 neurons in the *Gabbr1-cKO* cortex **(Fig. 3a; Extended Data Fig. 4c-e**). KEGG pathway
166 analysis of the differentially expressed genes (DEGs) in neurons revealed dysregulated
167 expression of GABAergic synapses, suggesting alterations in astrocyte-neuron
168 communication in the *Gabbr1-cKO* cortex **(Fig. 3b-c; Extended Table 3**).

169 To validate these findings, we quantified excitatory and inhibitory synapses in LI
170 and LII-II, respectively, from *Gabbr1-cKO* mice at P28. This analysis revealed an
171 increase in excitatory Vglut2/Psd95 synapses, coupled with no changes in the number
172 of inhibitory vGat/Gephrin synapses (**Extended Data Fig.5a-g)**. These changes in
173 synaptic numbers led us to evaluate whether loss of astrocytic *Gabbr1* influences
174 neuronal activity. Using intraventricular injection of AAV2/9-mDlx-mRuby2 at P1 to label
175 interneurons in *Gabbr1-cKO* and control mice (**Fig. 3d**), we evaluated neuronal
176 excitability, finding no differences in action potential firing between cKO and control
177 groups (**Extended Data Fig. 6b-i**). Next, we measured synaptic transmission through

bioRxiv preprint doi: https://doi.org/10.1101/2023.03.14.532493; this version posted March 15, 2023. The copyright holder for this preprint (which was not certified by peer review) is the author/funder, who has granted bioRxiv a license to display the preprint in perpetuity. It is made available under aCC-BY-NC-ND 4.0 International license.

178 spontaneous excitatory postsynaptic current/inhibitory postsynaptic current
179 (sEPSC/IPSC) finding dysregulation of both excitatory and inhibitory activity in LII-LIII
180 neurons. Excitatory neurons exhibited decreased sEPSC activity via cell average and K-
181 S test, while exhibiting no significant difference in sIPSC activities in cell averages and a
182 significant difference via K-S test (**Fig. 3e-f**). Analysis of inhibitory neurons revealed
183 increased sEPSC amplitudes and decreased sIPSC amplitudes via K-S test, which
184 were not statistically significant when averaged across cells (**Fig. 3g-h**). Next, we
185 subjected the *Gabbr1-cKO* (and control) mice to a series of behavioral tests, identifying
186 deficits in pre-pulse inhibition and three-chamber social interaction in the *Gabbr1-cKO*
187 mice (**Fig.3i-j**; **Extended Data Fig.5h-m**). Collectively, these molecular, physiological,
188 and behavioral data indicate that astrocytic *Gabbr1* mediates interactions with excitatory
189 and inhibitory neurons that contributes to functioning cortical circuits.
190

191 ***Gabbr1* regulates *Ednrb1* during astrocyte morphogenesis**

192 To identify the mechanisms downstream of *Gabbr1* regulating astrocyte morphogenesis
193 we performed bulk RNA-Seq on FACS purified astrocytes from P28 *Gabbr1-cKO* mice
194 from the cortex, hippocampus, olfactory bulb (**Fig.4a; Extended Tables 4**). Gene
195 Ontology (GO) analysis of the DEGs in *cKO* astrocytes highlighted extra-cellular matrix
196 and membrane-associated genes as the most represented across these regions
197 (**Fig.4b-c**). From this group, we focused on Endothelial Receptor B (*Ednrb*) and
198 confirmed reduced expression in astrocytes from the *Gabbr1-cKO* mouse (**Fig.4d-e).**
199 *Ednrb* is a GPCR that regulates cytoskeletal dynamics through Ca^{2+} activity and actin
200 organization in astrocytes[23,24] and contributes to reactive astrocyte responses after

bioRxiv preprint doi: https://doi.org/10.1101/2023.03.14.532493; this version posted March 15, 2023. The copyright holder for this preprint (which was not certified by peer review) is the author/funder, who has granted bioRxiv a license to display the preprint in perpetuity. It is made available under aCC-BY-NC-ND 4.0 International license.

201 brain injury[25], however its role in astrocyte morphogenesis is unknown. To examine
202 whether *Ednrb* regulates astrocyte morphogenesis, we employed the *Rosa-LSL-Cas9-*
203 *eGFP* mouse line, along with AAV-approaches to express Cas9 in astrocytes and
204 guideRNAs targeting *Ednrb* (**Fig.4f)**, which enabled selective deletion of *Ednrb* in
205 cortical astrocytes (**Fig.4g-i and Extended Data Fig.10b,f).** Using the mCherry tag on
206 the AAV-GFAP-Cre virus to assess morphology in astrocytes that had lost *Ednrb*, we
207 found a reduction in morphological complexity (**Fig.4g-i**). These findings highlight a new
208 role for *Ednrb* in astrocyte morphogenesis in the cortex and identify molecular
209 processes that act downstream of *Garbbr1*.
210

211 **Region-specific regulation of *Gabbr1***

212 To understand how *Gabbr1* fits into astrocytic developmental programs, we sought to
213 define the transcriptional mechanisms that control its expression. Our astrocyte
214 transcriptomic dataset from P1-P14 in the developing brain revealed temporal and
215 region-specific differences in gene expression profiles between the cortex,
216 hippocampus, and OB (**Extended Data Fig. 2a-d; Extended Table 1**), suggesting
217 region-specific mechanisms may regulate Gabbr1 expression. This prompted us to
218 perform Homer motif analysis on the DEGs between P1 and P14, identifying numerous
219 transcription factors (TFs) whose motifs are enriched from each region (**Fig. 5a**). Next,
220 we filtered these candidate TFs based on their expression levels, which nominated *Nfia*
221 *and Sox2* in the cortex, *Sox9* and *Nr2f1* in the hippocampus, and *Sox9* and *Tead1* in the
222 OB (**Fig. 5a, Extended Data Fig. 2a-c**).

bioRxiv preprint doi: https://doi.org/10.1101/2023.03.14.532493; this version posted March 15, 2023. The copyright holder for this preprint (which was not certified by peer review) is the author/funder, who has granted bioRxiv a license to display the preprint in perpetuity. It is made available under aCC-BY-NC-ND 4.0 International license.

223 To determine whether SOX9 and NFIA regulate *Gabbr1* in developing astrocytes
224 we utilized *Nfia$^{fl/fl}$; Aldh1l1-CreER; Aldh1l1-GFP* (*NFIA-cKO*) and *Sox9$^{fl/fl}$; Aldh1l1-*
225 *CreER; Aldh1l1-GFP* (*Sox9-cKO*) mouse lines that enable temporal control of deletion
226 in astrocytes[26,27]. To delete *Sox9* or *Nfia* during astrocyte morphogenesis, we treated
227 the above mouse lines (and *Nfia$^{fl/fl}$*; *Aldh1l1-GFP* or *Sox9$^{fl/fl}$*; *Aldh1l1-GFP* controls) with
228 a single injection of tamoxifen at P1 (**Fig. 5b**); analysis at P7 and P28 revealed efficient
229 knockout (**Extended Data Fig. 7a-d**). RNAscope analysis of *NFIA-cKO* mice revealed
230 that *Gabbr1* is specifically downregulated in Aldh1l1-GFP astrocytes from the cortex,
231 but not the OB (**Fig. 5c-e**). Conversely, in the *Sox9-cKO*, we found that *Gabbr1* is
232 downregulated in Aldh1l1-GFP astrocytes from the OB and not the cortex (**Fig. 5c, f-g**).
233 Next, we examined whether NFIA and SOX9 are sufficient to induce *Gabbr1*
234 expression, finding that NFIA overexpression in the cortex resulted in increased *Gabbr1*
235 expression, while SOX9 promotion of *Gabbr1* expression in the OB was not significant
236 (**Extended Data Fig. 7g-h**). To determine if *Gabbr1* is a direct target of NFIA and
237 SOX9, we performed chromatin immunoprecipitation PCR (ChIP-PCR) for the NFIA or
238 SOX9 binding motifs from P28 cortex and olfactory bulb, respectively (**Fig. 5h**). These
239 ChIP-PCR assays revealed that NFIA and SOX9 bind to their sites in the *Gabbr1*
240 promoter in the cortex and OB. Together, these data indicate region-specific regulation
241 of *Gabbr1* by NFIA and SOX9 in the cortex and OB, respectively.

242 To test whether GABA-induced $Ca2^{+}$ responses are impaired in the cortex of the
243 *Nfia-cKO* or OB of the *Sox9-cKO*, we used GCaMP6s and measured $Ca2^{+}$ activity in
244 astrocytes using ex-vivo, two photon imaging. Application of baclofen, the $GABA_B$
245 receptor agonist, revealed that cortical astrocytes from the *Nfia-cKO* and OB astrocytes

bioRxiv preprint doi: https://doi.org/10.1101/2023.03.14.532493; this version posted March 15, 2023. The copyright holder for this preprint (which was not certified by peer review) is the author/funder, who has granted bioRxiv a license to display the preprint in perpetuity. It is made available under aCC-BY-NC-ND 4.0 International license.

246 from the *Sox9-cKO* failed to generate a baclofen-induced $Ca2^{+}$ response (**Fig. 5i-j**;
247 **Extended Data Fig. 7e-f**). These observations indicate that *Gabbr1* responses are
248 impaired in *Nfia* and *Sox9* mutant astrocytes from the cortex and OB, respectively,
249 further region-specific regulation of *Gabbr1* expression.
250
251 **Region-specific regulation of astrocyte morphogenesis**
252 *Sox9* and *Nfia* play an important role in early glial specification in the embryonic spinal
253 cord, however whether they regulate astrocyte morphogenesis in the brain is
254 unknown[28–30]. Recent studies have also shown that despite universal expression in
255 astrocytes, *Sox9* is required to maintain astrocyte complexity in the adult olfactory bulb,
256 while *Nfia* is required to maintain astrocyte complexity in the adult hippocampus and
257 adult cortex[26,27]. However, whether these region-specific transcriptional dependencies in
258 the adult are developmentally encoded remains unknown.
259 To determine whether *Sox9* and *Nfia* regulate astrocyte morphogenesis in a
260 region-specific manner we harvested *Sox9-cKO* and *Nfia-cKO* (and controls) at P28.
261 Our initial analysis found no changes in proliferation or gross number of Aldh1l1-GFP
262 astrocytes at P28 in the cortex and OB in both the *Nfia-cKO* and *Sox9-cKO* mice,
263 respectively (**Extended Data Fig. 8e-h**). To evaluate the morphological complexity of
264 astrocytes from the *Nfia-cKO* and *Sox9-cKO* we focused on layer II-III (LII-LIII) of the
265 visual cortex, external plexiform layer (EPL) OB, and CA1 in the hippocampus. We
266 found that knockout of *Sox9* led to a reduction in astrocyte complexity in the OB,
267 whereas astrocytes in the cortex or hippocampus are unaffected (**Fig. 6a-b, Extended**
268 **Data Fig. 8b,d**). In contrast, knockout of *Nfia* led to a reduction in astrocyte complexity

bioRxiv preprint doi: https://doi.org/10.1101/2023.03.14.532493; this version posted March 15, 2023. The copyright holder for this preprint (which was not certified by peer review) is the author/funder, who has granted bioRxiv a license to display the preprint in perpetuity. It is made available under aCC-BY-NC-ND 4.0 International license.

269 in the hippocampus and cortex, but not the OB (**Fig. 6a-b, Extended Data Fig. 8a,c).**
270 These data indicate that region-specific transcriptional dependencies regulate astrocyte
271 morphogenesis during development.

272 These studies highlight a possible role for *Nfia* in the development and function
273 of cortical circuits. To interrogate synapse formation we quantified excitatory and
274 inhibitory synapses in LI and LII-II, finding no changes in the number of vGlut2/Psd95,
275 vGat/Gephyrin, or vGlut1/Psd95 puncta from *NFIA-cKO* mice (**Extended Data Fig. 9a-**
276 **d**). Measuring synaptic transmission through spontaneous excitatory postsynaptic
277 current/inhibitory postsynaptic current (sEPSC/IPSC), we found decreases in
278 sEPSC/IPSC in both excitatory and inhibitory neurons in LII-III via K-S test that were not
279 statistically significant when averaged across cells; sIPSC of inhibitory neurons
280 demonstrated significant decreases via K-S test and across cell averages (**Extended**
281 **Data Fig.9e-f**). Next, we subjected these mice to a series of behavioral assays finding
282 specific defects in pre-pulse inhibition and three-chamber social interaction (**Extended**
283 **Data Fig. 9g-h;k-p**), deficits that parallel our observations in the *Gabbr1-cKO* mouse
284 line (**Fig.3j**). Collectively, these data indicate that astrocytic NFIA contributes to the
285 development of cortical circuits and implicates astrocyte morphogenesis as a central
286 component of circuit maturation.
287

288 **LHX2 cooperates with NFIA to regulate cortical astrocyte morphogenesis**

289 Because NFIA and SOX9 exhibit universal expression in astrocytes and have region-
290 specific roles, led us to examine how this regional specialization is conferred.
291 Identification of region-specific transcriptional mechanisms may reveal insights into the

bioRxiv preprint doi: https://doi.org/10.1101/2023.03.14.532493; this version posted March 15, 2023. The copyright holder for this preprint (which was not certified by peer review) is the author/funder, who has granted bioRxiv a license to display the preprint in perpetuity. It is made available under aCC-BY-NC-ND 4.0 International license.

292 regional regulation of astrocyte morphogenesis and *Gabbr1* expression during
293 development. Analysis of regional and temporal signatures from our developing
294 astrocyte RNA-Seq data (**Extended Data Fig. 2a-c**) revealed a cohort of TFs
295 expressed in cortical or olfactory bulb astrocytes (**Figs.6c,f, Extended data table 5**).
296 We found that the transcription factor *Lhx2* is expressed in cortical astrocytes, while the
297 transcription factor *Npas3* is expressed in olfactory bulb astrocytes (**Fig.6d,g**). We
298 previously demonstrated that hippocampal-specific functions of NFIA in the adult are
299 mediated by interactions with other transcription factors[26], therefore we examined
300 whether LHX2 and NPAS3 interact with NFIA or SOX9, respectively. Towards this we
301 performed a series of co-immunoprecipitation experiments, finding that NFIA associates
302 with LHX2 in the cortex, while NPAS3 associates with SOX9 in the olfactory bulb
303 (**Fig.6e,h**).

304 Prior studies on *Lhx2* suggest that it has a region-specific role in the embryonic
305 brain, where it promotes neurogenesis in the hippocampus by antagonizing NFIA
306 function[31]. Interestingly, *Lhx2* does not promote neurogenesis in the cortex and its role
307 in astrocyte development remains unknown. Using the *Rosa-LSL-Cas9-eGFP* mouse
308 line, along with AAV-approaches to delete *Lhx2* we found that its loss resulted in
309 decreased morphological complexity (**Fig.6j-l and Extended Data Fig. 10c,g**). Given its
310 biochemical relationship with NFIA and its role in astrocyte morphogenesis, we
311 determined whether loss of *Lhx2* affects *Gabbr1* expression. To evaluate *Gabbr1*
312 expression we used RNAscope, finding that its expression is significantly reduced in
313 astrocytes that have lost *Lhx2* **(Fig.6m**). These data illustrate a role for *Lhx2* in

bioRxiv preprint doi: https://doi.org/10.1101/2023.03.14.532493; this version posted March 15, 2023. The copyright holder for this preprint (which was not certified by peer review) is the author/funder, who has granted bioRxiv a license to display the preprint in perpetuity. It is made available under aCC-BY-NC-ND 4.0 International license.

314 promoting astrocyte morphogenesis, and indicates that Lhx2 cooperates with NFIA to
315 regulate *Gabbr1* expression and drive morphogenesis in developing cortical astrocytes.
316

317 **Discussion**

318 The cellular and molecular mechanisms by which neuronal input contributes to
319 astrocyte development are fundamental questions. In this study, we demonstrate that
320 astrocyte morphogenesis in the developing cortex is driven by the activity of inhibitory
321 neurons. We further show that deletion of *Gabbr1*, a GABA receptor, in astrocytes
322 results in defective morphogenesis, indicating that it functions as a central regulator of
323 astrocytogenesis. Mechanistically, the link between *Gabbr1* and *Ednrb* reveals new
324 insights into how inhibitory inputs drive signaling pathways that remodel cellular
325 architecture associated with morphology[23,24]. Endothelin ligands[32] are released by
326 several cellular sources, further highlighting the role of cell-cell communication as a
327 central driver of astrocyte morphology. Similar to activity-dependent myelination[33–35],
328 our results indicate that inhibitory neurons provide cues that drive astrocyte
329 development, they also suggest that other forms of activity-dependent input contribute
330 to astrocyte maturation, including excitatory neurons. Given the proximity of peripheral
331 astrocyte processes to neuronal synapses, a model emerges, where astrocyte
332 morphogenesis is likely tuned to the activity of the surrounding neuronal milieu or
333 neurons from a common ancestral origin.

334 Our finding that *Gabbr1* exhibits region-specific regulation by SOX9 and NFIA,
335 places it as part of the transcriptional program driving astrocytogenesis. Furthermore,
336 we identified new roles for Sox9 and NFIA in astrocyte morphogenesis in the brain,

bioRxiv preprint doi: https://doi.org/10.1101/2023.03.14.532493; this version posted March 15, 2023. The copyright holder for this preprint (which was not certified by peer review) is the author/funder, who has granted bioRxiv a license to display the preprint in perpetuity. It is made available under aCC-BY-NC-ND 4.0 International license.

337 while establishing a new mechanism by which these transcription factors enable
338 developing astrocytes to respond to neuronal cues. Critically, these findings highlight
339 region-specific mechanisms of astrocyte development, where the OB requires SOX9,
340 while the cortex and hippocampus require NFIA. Parallel observations were made in
341 adult astrocytes, indicating that these region-specific transcriptional dependencies in the
342 adult are developmentally encoded[26,27]. Our studies suggest a mechanism by which
343 transcription factors with region restricted patterns of expression (i.e. LHX2 and NPAS3)
344 confer the regional dependency of ubiquitously expressed transcription factors (i.e.
345 NFIA and SOX9). Together, this suggests a combinatorial transcription factor code, akin
346 to pattern formation, that operates in a region-specific manner to oversee astrocyte
347 development and function.
348
349
350 **Acknowledgements**
351
352 This work was supported by US National Institutes of Health grants NS071153,
353 AG071687, and NS096096 to BD. We are thankful for support from the David and Eula
354 Wintermann Foundation. We thank Bernhard Bettler for providing the *Gabbr1*-floxed
355 mouse line. scRNA-Seq studies were performed at the Single Cell Genomics Core at
356 BCM partially supported by NIH shared instrument grants (S10OD023469,
357 S10OD025240) and P30EY002520. This project was supported by the Cytometry and
358 Cell Sorting Core at Baylor College of Medicine with funding from the CPRIT Core
359 Facility Support Award (CPRIT-RP180672), the NIH (CA125123 and RR024574) and
360 the assistance of Joel M. Sederstrom. Research reported in this publication was
361 supported by the Eunice Kennedy Shriver National Institute of Child Health & Human

bioRxiv preprint doi: https://doi.org/10.1101/2023.03.14.532493; this version posted March 15, 2023. The copyright holder for this preprint (which was not certified by peer review) is the author/funder, who has granted bioRxiv a license to display the preprint in perpetuity. It is made available under aCC-BY-NC-ND 4.0 International license.

362 Development of the National Institutes of Health under Award Number P50HD103555
363 for use of the Microscopy Core facilities and the Animal Phenotyping & Preclinical
364 Endpoints Core facilities.

365

366 **Authors Contributions**

367

368 YTC and BD conceived the project and designed the experiments; YTC, JW, ZFL and
369 ELF performed the experiments; JW executed the electrophysiology studies; YTC and
370 ASH designed and executed the bioinformatics analyses. YTC and BD wrote the
371 manuscript.

372

373 **Competing interests**

374 The authors declare no competing interests.

375

376 **References**

377

378 1. Allen, N. J. Astrocyte Regulation of Synaptic Behavior. *Annu. Rev. Cell Dev. Biol.* 30,
379 439–463 (2014).

380 2. Khakh, B. S. & Deneen, B. The Emerging Nature of Astrocyte Diversity. *Annu Rev*
381 *Neurosci* 42, 187–207 (2019).

382 3. Volterra, A. & Meldolesi, J. Astrocytes, from brain glue to communication elements:
383 the revolution continues. *Nat Rev Neurosci* 6, 626–640 (2005).

384 4. Bushong, E. A., Martone, M. E., Jones, Y. Z. & Ellisman, M. H. Protoplasmic
385 Astrocytes in CA1 Stratum Radiatum Occupy Separate Anatomical Domains. *J*
386 *Neurosci* 22, 183–192 (2002).

387 5. Molofsky, A. V. *et al.* Astrocytes and disease: a neurodevelopmental perspective.
388 *Genes Dev.* 26, 891–907 (2012).

389 6. Seifert, G., Schilling, K. & Steinhäuser, C. Astrocyte dysfunction in neurological
390 disorders: a molecular perspective. *Nat Rev Neurosci* 7, 194–206 (2006).

bioRxiv preprint doi: https://doi.org/10.1101/2023.03.14.532493; this version posted March 15, 2023. The copyright holder for this preprint (which was not certified by peer review) is the author/funder, who has granted bioRxiv a license to display the preprint in perpetuity. It is made available under aCC-BY-NC-ND 4.0 International license.

391 7. Pekny, M. *et al.* Astrocytes: a central element in neurological diseases. *Acta*
392 *Neuropathol* 131, 323–345 (2016).

393 8. Clarke, L. E. & Barres, B. A. Emerging roles of astrocytes in neural circuit
394 development. *Nat Rev Neurosci* 14, 311–321 (2013).

395 9. Allen, N. J. & Eroglu, C. Cell Biology of Astrocyte-Synapse Interactions. *Neuron* 96,
396 697–708 (2017).

397 10. Farhy-Tselnicker, I. *et al.* Activity-dependent modulation of synapse-regulating
398 genes in astrocytes. *Elife* 10, e70514 (2021).

399 11. Stogsdill, J. A. *et al.* Astrocytic neuroligins control astrocyte morphogenesis and
400 synaptogenesis. *Nature* 551, 192–197 (2017).

401 12. Müller, C. M. Dark-rearing retards the maturation of astrocytes in restricted layers of
402 cat visual cortex. *Glia* 3, 487–494 (1990).

403 13. Morel, L., Higashimori, H., Tolman, M. & Yang, Y. VGluT1+ Neuronal Glutamatergic
404 Signaling Regulates Postnatal Developmental Maturation of Cortical Protoplasmic
405 Astroglia. *J Neurosci* 34, 10950–10962 (2014).

406 14. Lin, C.-C. J. *et al.* Identification of diverse astrocyte populations and their malignant
407 analogs. *Nature Publishing Group* 20, 1–13 (2017).

408 15. Anthony, T. E. & Heintz, N. The folate metabolic enzyme ALDH1L1 is restricted to
409 the midline of the early CNS, suggesting a role in human neural tube defects. *J Comp*
410 *Neurol* 500, 368–383 (2007).

411 16. Dimidschstein, J. *et al.* A viral strategy for targeting and manipulating interneurons
412 across vertebrate species. *Nat Neurosci* 19, 1743–1749 (2016).

413 17. Bettler, B., Kaupmann, K., Mosbacher, J. & Gassmann, M. Molecular Structure and
414 Physiological Functions of GABAB Receptors. *Physiol Rev* 84, 835–867 (2004).

415 18. Wu, C. & Sun, D. GABA receptors in brain development, function, and injury. *Metab*
416 *Brain Dis* 30, 367–379 (2015).

417 19. Srinivasan, R. *et al.* New Transgenic Mouse Lines for Selectively Targeting
418 Astrocytes and Studying Calcium Signals in Astrocyte Processes In Situ and
419 In Vivo. *Neuron* 92, 1181–1195 (2016).

420 20. Mariotti, L., Losi, G., Sessolo, M., Marcon, I. & Carmignoto, G. The inhibitory
421 neurotransmitter GABA evokes long-lasting Ca 2+oscillations in cortical astrocytes. *Glia*
422 64, 363–373 (2015).

bioRxiv preprint doi: https://doi.org/10.1101/2023.03.14.532493; this version posted March 15, 2023. The copyright holder for this preprint (which was not certified by peer review) is the author/funder, who has granted bioRxiv a license to display the preprint in perpetuity. It is made available under aCC-BY-NC-ND 4.0 International license.

423 21. Hao, Y. *et al.* Integrated analysis of multimodal single-cell data. *Cell* 184, 3573-
424 3587.e29 (2021).

425 22. Jin, S. *et al.* Inference and analysis of cell-cell communication using CellChat. *Nat*
426 *Commun* 12, 1088 (2021).

427 23. Koyama, Y., Yoshioka, Y., Hashimoto, H., Matsuda, T. & Baba, A. Endothelins
428 increase tyrosine phosphorylation of astrocytic focal adhesion kinase and paxillin
429 accompanied by their association with cytoskeletal components. *Neuroscience* 101,
430 219–227 (2000).

431 24. Koyama, Y. Endothelin ETB Receptor-Mediated Astrocytic Activation: Pathological
432 Roles in Brain Disorders. *Int J Mol Sci* 22, 4333 (2021).

433 25. Hammond, T. R. *et al.* Endothelin-B Receptor Activation in Astrocytes Regulates the
434 Rate of Oligodendrocyte Regeneration during Remyelination. *Cell Reports* 13, 2090–
435 2097 (2015).

436 26. Huang, A. Y.-S. *et al.* Region-Specific Transcriptional Control of Astrocyte Function
437 Oversees Local Circuit Activities. *Neuron* 1–27 (2020)
438 doi:10.1016/j.neuron.2020.03.025.

439 27. Ung, K. *et al.* Olfactory bulb astrocytes mediate sensory circuit processing through
440 Sox9 in the mouse brain. *Nature Communications* 1–15 (2021) doi:10.1038/s41467-
441 021-25444-3.

442 28. Deneen, B. *et al.* The Transcription Factor NFIA Controls the Onset of Gliogenesis
443 in the Developing Spinal Cord. *Neuron* 52, 953–968 (2006).

444 29. Kang, P. *et al.* Sox9 and NFIA Coordinate a Transcriptional Regulatory Cascade
445 during the Initiation of Gliogenesis. *Neuron* 74, 79–94 (2012).

446 30. Stolt, C. C. *et al.* The Sox9 transcription factor determines glial fate choice in the
447 developing spinal cord. *Genes Dev.* 17, 1677–1689 (2003).

448 31. Subramanian, L. *et al.* Transcription factor Lhx2 is necessary and sufficient to
449 suppress astrogliogenesis and promote neurogenesis in the developing hippocampus.
450 *Proc National Acad Sci* 108, E265–E274 (2011).

451 32. KUWAKI, T. *et al.* PHYSIOLOGICAL ROLE OF BRAIN ENDOTHELIN IN THE
452 CENTRAL AUTONOMIC CONTROL: FROM NEURON TO KNOCKOUT MOUSE. *Prog*
453 *Neurobiol* 51, 545–579 (1997).

454 33. Gibson, E. M. *et al.* Neuronal Activity Promotes Oligodendrogenesis and Adaptive
455 Myelination in the Mammalian Brain. *Science* 344, 1252304 (2014).

bioRxiv preprint doi: https://doi.org/10.1101/2023.03.14.532493; this version posted March 15, 2023. The copyright holder for this preprint (which was not certified by peer review) is the author/funder, who has granted bioRxiv a license to display the preprint in perpetuity. It is made available under aCC-BY-NC-ND 4.0 International license.

456 34. Baraban, M., Koudelka, S. & Lyons, D. A. Ca2+ activity signatures of myelin sheath
457 formation and growth in vivo. *Nat Neurosci* 21, 19–23 (2018).

458 35. Osso, L. A., Rankin, K. A. & Chan, J. R. Experience-dependent myelination
459 following stress is mediated by the neuropeptide dynorphin. *Neuron* 109, 3619-3632.e5
460 (2021).

461

462 **Figure Legends**

463

464 **Figure 1. Inhibitory neuron activity regulates astrocyte morphogenesis**

465 **a.** Schematic of DREADD-based activation of inhibitory neurons in post-natal Aldh1l1-
466 GFP mice. **b.** Slice electrophysiological recordings of DREADD-expressing (hM3Dq or
467 hM4Di) inhibitory neurons at P21, with and without CNO activation. Traces are
468 representative of neuronal firing. **c-e.** Imaging of Aldh1l1-GFP astrocytes after hM3Dq
469 activation of inhibitory neurons; quantification using Scholl analysis, branch number,
470 and total processes at P21; $n = 3$ pairs of animals (47, 51 cells; **d**, generalized linear
471 mixed-effects (GLME) model with Sidak's multiple comparisons test, $^{**}P = 0.001$; **e**,
472 linear mixed-effect (LME) model, $^{***}P = 0.00012, 0.00013$). **f.** RNAscope imaging and
473 quantitative analysis for *Gabbr1* expression in Alhd1l1-GFP expressing astrocytes at
474 P21; $n = 3$ pairs of animals (49, 59 cells; LME model, $^{***}P = 0.00090$). Dashed circle
475 denotes astrocyte with *Gabbr1*. **g-i.** Imaging of Aldh1l1-GFP astrocytes after hM4Di
476 inhibition of inhibitory neurons; quantification using Scholl analysis, branch number, and
477 total processes at P21; $n = 3$ and 4 animals (44, 71 cells; **h**, GLME model with Sidak's
478 multiple comparisons test, $^{**}P = 0.0013$; **i-j**, GLME model, $^{*}P = 0.0327$, $^{**}P = 0.0014$). **j.**
479 RNAscope imaging and quantitative analysis for *Gabbr1* expression in Alhd1l1-GFP
480 expressing astrocytes at P21; $n = 3$ and 4 animals (49, 64 cells; LME model, $P =$

bioRxiv preprint doi: https://doi.org/10.1101/2023.03.14.532493; this version posted March 15, 2023. The copyright holder for this preprint (which was not certified by peer review) is the author/funder, who has granted bioRxiv a license to display the preprint in perpetuity. It is made available under aCC-BY-NC-ND 4.0 International license.

481 0.1014). Dashed circle denotes astrocyte with *Gabbr1*. Scale bars, 20 μm (**c**, **g**, **j**) and
482 10 μm (**f**). Data represent mean ± s.d. (**d**, **h**), median, minimum value, maximum value
483 and interquartile range (IQR) (**e-f** bottom, **i-j**).
484

485 **Figure 2. *Gabbr1* is required for astrocyte morphogenesis**

486 **a.** Experimental timeline and mouse lines rendering astrocyte-specific knockout of
487 *Gabbr1*. **b.** RNA-Scope imaging of *Gabbr1* within Aldh1l1-GFP astrocytes from control
488 and *Gabbr1-cKO* mouse lines; quantification derived from $n = 3$ pairs of animals
489 (*control*: OB 18, CX 18, HC 16; *cKO*: OB 17, CX 19, HC 17 cells; LME model, ***P =
490 0.00020, ****P = 3.07e-06, **P = 0.0030). Dashed circle denotes astrocyte with *Gabbr1*.
491 **c.** Imaging of Aldh1l1-GFP astrocytes from the cortex, CA1 of the hippocampus, and
492 olfactory bulb at P28; quantification via Scholl analysis derived from $n = 3$ pairs of
493 animals (*control*: OB 43, CX 27, HC 32, *cKO*: OB 31, CX 33, HC 30 cells; GLME model
494 with Sidak's multiple comparisons test, **P = 0.0011, *** P = 0.0006, **P = 0.0037). **d.**
495 Imaging of GCaMP6s activity in *control* and *Gabbr1-cKO* astrocytes from the cortex at
496 P28; quantification is derived from $n = 3$ pairs of animals (24,33 cells; GLME model, P =
497 0.6361, 0.2239). **e.** Imaging of GCaMP6s activity in the presence of TTX and baclofen;
498 quantification derived from $n = 40$ cells from 3 pairs of animals (two-tailed Wilcoxon
499 matched-pairs signed rank test, *P = 0.022, P = 0.89, ***P = 0.0006, P = 0.32). **f.**
500 DREADD-based activation of inhibitory neurons in *Gabbr1-cKO* mice. **g-i.** Imaging of
501 Aldh1l1-GFP astrocytes from *Gabbr1-cKO* (and *control*) after hM3Dq activation of
502 inhibitory neurons; quantification using Scholl analysis, branch number, and total
503 processes at P21; $n = 3$ and 5 animals (50, 80 cells; **h**, GLME model with Sidak's

bioRxiv preprint doi: https://doi.org/10.1101/2023.03.14.532493; this version posted March 15, 2023. The copyright holder for this preprint (which was not certified by peer review) is the author/funder, who has granted bioRxiv a license to display the preprint in perpetuity. It is made available under aCC-BY-NC-ND 4.0 International license.

504 multiple comparisons test, ***P* = 0.0011, **i**; GLME model, **P* = 0.034, ***P* = 0.0026).
505 Scale bars, 10 µm (**b, d**), 30 µm (**c**), and 20 µm (**g**). Data represent mean ± s.d. (**c**, **h**),
506 median, minimum value, maximum value and IQR (**b**, **d**, **i**).
507

508 **<u>Figure 3. Loss of astrocytic *Gabbr1* disrupts cortical circuit function</u>**

509 **a.** CellChat interaction diagram illustrating astrocyte interactions with neurons in the
510 cortex from P28 *Gabbr1-cKO* mice; width of colored arrow indicates scale of interaction.
511 See Extended Data Figure 4. **b-c**. KEGG pathway analysis of neurons from *Gabbr1-*
512 *cKO* scRNA-Seq (**b**, analyzed by Enrichr) and dot plot of differentially expressed genes
513 from KEGG (**c**, analyzed by Seurat FindMarkers). **d.** Schematic of viral labeling of
514 inhibitory neurons and experimental timeline. **e-h.** Representative traces of
515 spontaneous EPSCs and IPSCs from excitatory and inhibitory neurons from cortex of
516 *Gabbr1-cKO* and *controls*. Associated cumulative and bar plots demonstrate
517 quantification of sEPSC and sIPSC from 3 pairs of animals (**e**, *n* = 13, 15 cells;
518 Kolmogorov-Smirnov test, **** *P* < 0.0001; two-tailed Mann-Whitney test, *P* = 0.8207,
519 ***P* = 0.003; **f**, *n* = 15, 12 cells; Kolmogorov-Smirnov test, **** *P* < 0.0001; two-tailed
520 Mann-Whitney test, *P* = 0.1995, 0.5888; **g**, *n* = 13, 15 cells; Kolmogorov-Smirnov test,
521 **** *P* < 0.0001; two-tailed Mann-Whitney test, *P* = 0.7856, 0.0504; **h**, *n* = 11, 9 cells;
522 Kolmogorov-Smirnov test, **** *P* < 0.0001; two-tailed Mann-Whitney test, *P* = 0.2299,
523 0.3796). **i.** Experimental timeline for behavioral analysis. **j**. 3-chamber social interaction
524 and pre-pulse inhibition studies on *Gabbr1-cKO* and *control* mice from 10 animals in
525 control group and 11 animals in cKO group (left, GLME model with Sidak's multiple

bioRxiv preprint doi: https://doi.org/10.1101/2023.03.14.532493; this version posted March 15, 2023. The copyright holder for this preprint (which was not certified by peer review) is the author/funder, who has granted bioRxiv a license to display the preprint in perpetuity. It is made available under aCC-BY-NC-ND 4.0 International license.

526 comparisons test, **P* = 0.015; right, two-tailed Mann-Whitney test, **P* = 0.043). Data
527 represent mean ± s.e.m. (**e-h**), s.d. (**j**).
528
529
530
531 **Figure 4. *Gabbr1* regulates astrocyte morphology through *Ednrb1***
532 **a.** Volcano plots from RNA-Seq analysis of control and *Gabb1-cKO* astrocytes from
533 cortex, hippocampus, and OB. **b.** Table of the number of differentially expressed genes
534 (DEGs) from each region. **c.** Gene Ontology (GO) analysis of DEGs performed with
535 Enrichr. **d.** Immunostaining for EDNRB in P28 astrocytes from *Gabbr1-cKO* and *control*
536 astrocytes. **e.** Quantification of EDNRB expression in *Gabbr1-cKO* and control from *n* =
537 6 pairs of animals (two-tailed Mann-Whitney test, **P* = 0.041, 0.015, *P* = 0.1320). **f.**
538 Schematic and timeline of selective deletion of *Ednrb* in cortical astrocytes. **g-i.** Imaging
539 of virally labeled astrocytes from the P28 cortex of mice where *Ednrb* has been knocked
540 out using guideRNAs in the *ROSA-LSL-Cas9-EGFP* mouse line; quantification via
541 Scholl analysis was derived from *n* = 3 pairs of animals (53, 49 cells; **h**, GLME model
542 with Sidak's multiple comparisons test, ***P* = 0.001; i, GLME model, ***P* = 0.001, ****P* =
543 0.0002). Scale bars, 20 µm (**d**), 30 µm (**g**). Data represent mean ± s.d. (**h**), median,
544 minimum value, maximum value and IQR (**e**, **i**).
545
546
547
548

bioRxiv preprint doi: https://doi.org/10.1101/2023.03.14.532493; this version posted March 15, 2023. The copyright holder for this preprint (which was not certified by peer review) is the author/funder, who has granted bioRxiv a license to display the preprint in perpetuity. It is made available under aCC-BY-NC-ND 4.0 International license.

549
550
551
552
553
554 **Figure 5. Region-specific regulation of *Gabbr1* by SOX9 and NFIA**

555 **a.** Homer transcription factor motif analysis on differentially expressed genes (DEGs)
556 from P1 and P14 timepoints from astrocytes isolated from the cortex, hippocampus, and
557 olfactory bulb. **b.** Schematic depicting mouse lines and experimental timelines. **c-h.**
558 RNAscope imaging of *Gabbr1* expression in Aldh1l1-GFP astrocytes from *Nfia-cKO*,
559 *Sox9-cKO* and associated controls at P28; quantitative analysis of *Gabbr1* expression is
560 derived from n = 3 pairs of animals (**d**, 50, 50, 29, and 33 cells; GLME model, *P =
561 0.022; LME model ***P = 0.0002; **e**, 29, 19, 19, and 25 cells; LME model, P = 0.17,
562 0.27; **f**, 26, 25, 26, and 29 cells; GLME model, P = 0.91, 0.95; **g**, 30, 29, 29, 30 cells;
563 LME model, **P = 0.0094, *P = 0.014). Dashed circle denotes astrocyte with *Gabbr1*. **h.**
564 Chromatin immunoprecipitation of NFIA from P28 cortex or SOX9 from P28 olfactory
565 bulb (OB), followed by PCR detection of association with motif in proximal promoter
566 region of *Gabbr1*. **i-j.** Imaging of GCaMP6s activity from the cortex of *Nfia-cKO* mice or
567 the OB from *Sox9-cKO* mice (and *controls*) in the presence of TTX and baclofen;
568 quantification is derived from n = 19-26 cells from 3 pairs of animals (**i**, 23, 26 cells, two-
569 tailed Wilcoxon matched-pairs signed rank test, ***P = 0.0001, P = 0.53, *P = 0.048, P =
570 0.37; **j**, 19 20 cells, two-tailed Wilcoxon matched-pairs signed rank test, P = 0.65, 0.45,

bioRxiv preprint doi: https://doi.org/10.1101/2023.03.14.532493; this version posted March 15, 2023. The copyright holder for this preprint (which was not certified by peer review) is the author/funder, who has granted bioRxiv a license to display the preprint in perpetuity. It is made available under aCC-BY-NC-ND 4.0 International license.

571 **P* = 0.012, *P* = 0.81). Scale bars, 10 μm (**c**) and 20 μm (**i-j**). Data represent median,
572 minimum value, maximum value and IQR (**d-g**).
573
574
575
576
577 **Figure 6. Regulation of astrocyte morphogenesis by region-specific mechanisms**
578 **a.** Timeline and mouse lines rendering astrocyte-specific knockout of *Sox9* and *Nfia*. **b.**
579 Imaging of Aldh1l1-GFP astrocytes at P28 from the *Sox9-cKO* and *Nfia-cKO*;
580 quantification via Scholl analysis was derived from *n* = 3 pairs of animals (*Nfia control*:
581 OB 56, CX 52, *Nfia cKO*: OB 60, CX 48, *Sox9 control*: OB 29, CX 35, *Sox9 cKO*: OB
582 39, CX 33 cells; GLME model with Sidak's multiple comparisons test, **P* = 0.015, *P* =
583 0.41, 0.60, ***P* = 0.0097). **c.** CX-specific DEGs increased between P7-P14. **d**.
584 Immunostaining for LHX2 in P28 astrocytes quantified from *n* = 3 pairs of animals (LME
585 model, *****P* = 1.31e-12). **e**. Immunoprecipitation of LHX2 and immunoblot of LHX2 and
586 NFIA from the P28 cortex. **f.** OB-specific DEGs increased between P7-P14. **g**.
587 Immunostaining for NPAS3 in P28 astrocytes quantified from *n* = 3 pairs of animals
588 (GLME model, ***P* = 0.0013). **h**. Immunoprecipitation of NPAS3 and immunoblot of
589 NPAS3 and SOX9 from P28 cortex. **i.** Schematic of *Lhx2* deletion in cortical astrocytes.
590 **j-l**. Imaging of virally labeled astrocytes lacking *Lhx2* from P28 cortex; quantification via
591 Scholl analysis was derived from *n* = 3 pairs of animals (41,41 cells; **k**, GLME model
592 with Sidak's multiple comparisons test, *****P* = 1.29e-24; **l**, GLME model, ****P* =
593 0.00099, *****P* = 3.98e-05). **m**. RNAscope for Gabbr1 expression in *Cas9-EGFP* cortical

bioRxiv preprint doi: https://doi.org/10.1101/2023.03.14.532493; this version posted March 15, 2023. The copyright holder for this preprint (which was not certified by peer review) is the author/funder, who has granted bioRxiv a license to display the preprint in perpetuity. It is made available under aCC-BY-NC-ND 4.0 International license.

594 astrocytes lacking *Lhx2* and controls at P28; quantitative analysis demonstrating
595 reduction of *Gabbr1* expression is derived from $n = 3$ pairs of animals (51,55 cells;
596 GLME model, **P* = 0.015; LME model, **P = 0.0003). Scale bars, 30 μm (**b, j**), 20 μm
597 (**d**, **g**, **m**). Data represent mean ± s.d. (**b**, **k**), median, minimum value, maximum value
598 and IQR (**d**, **g**, **l**, **m**).
599

600 **Methods**
601

602 **<u>Animals</u>**

603 All experimental animals were treated in compliance with the US Department of Health
604 and Human Services, the NIH guidelines, and Baylor College of Medicine IACUC
605 guidelines. All mice were housed with food and water available ad libitum in a 12-hour
606 light/dark, 20-22 degree, and 40-60% humidity environment. Both female and male mice
607 were used for all experiments, and littermates of the same sex were randomly allocated
608 to experimental groups. For ex vivo and in vivo experiments, P28 animals were used
609 unless otherwise described. All mice used in this study were maintained on the
610 C57BL/6J background. Different conditional knockout mice were generated by crossing
611 fl/fl mice with Aldh1l1-CreER (The Jackson Laboratory; RRID:IMSR JAX:029655). For
612 *Gabbr1* conditional knockout mice, *Gabbr1*$^{fl/fl}$ conditional mutant mice were crossed with
613 Aldh1l1-CreER, resulting in *Gabbr1*$^{fl/fl}$; Aldh1l1-CreER (*Gabbr1 cKO*) and *Gabbr1*$^{fl/fl}$
614 (*Gabbr1 control*) littermate controls[36]. For *Sox9* conditional knockout mice, *Sox9*$^{fl/fl}$
615 conditional mutant mice were crossed with Aldh1l1-CreER, resulting in *Sox9*$^{fl/fl}$; Aldh1l1-
616 CreER (*Sox9 cKO*) and *Sox9*$^{fl/fl}$ (*Sox9 control*) littermate controls[37]. For *Nfia* conditional
617 knockout mice, *Nfia*$^{fl/fl}$ conditional mutant mice were crossed with Aldh1l1-CreER,

bioRxiv preprint doi: https://doi.org/10.1101/2023.03.14.532493; this version posted March 15, 2023. The copyright holder for this preprint (which was not certified by peer review) is the author/funder, who has granted bioRxiv a license to display the preprint in perpetuity. It is made available under aCC-BY-NC-ND 4.0 International license.

618 resulting in *Nfia*$^{fl/fl}$; Aldh1l1-CreER (*Nfia cKO*) and *Nfia*$^{fl/fl}$ (*Nfia control*) littermate
619 controls[26]. For histological analysis, the Aldh1l1-GFP mouse was crossed with control or
620 knockout, resulting in cKO; Aldh1l1-GFP and control; Aldh1l1-GFP mice. For Ca2+
621 image analysis, Ai96 (RCL-GCaMP6s) mouse (The Jackson Laboratory;
622 RRID:IMSR_JAX:024106) were crossed with control of knockout. For Tdtomato
623 astrocyte labeling, Ai14 (RCL-Td) mouse (The Jackson Laboratory;
624 RRID:IMSR_JAX:007914) were crossed with control of cKO. To induce deletion of
625 *Gabbr1*, *Sox9*, or *Nfia* in developing astrocytes in the P28 brain, P0 pups were injected
626 subcutaneously with 100 mg/kg body weight of Tamoxifen (Sigma-Aldrich, cat no.
627 T5648) dissolved in a 9:1 corn oil/ethanol mixture for single injection at P0-P1. To
628 perform CRISPR-dependent tissue specific knockout of *Ednrb* and *Lhx2*, we utilized
629 Rosa26-LSL-Cas9 knockin mice (The Jackson Laboratory; RRID:IMSR_JAX: 026175).
630 To conditionally knock out *Ednrb* and *Lhx2*, we intraventricularly injected AAV2/9 GFAP-
631 Cre and AAV2/9 U6-sgRNA-GFAP-mCherry into P0-P1 Rosa26-LSL-Cas9
632 heterozygous and wild-type littermates. Four weeks after injection, we collected the
633 brain, confirmed the expression of EDNRB or LHX2 through immunofluorescence
634 staining, and performed astrocyte morphological analysis and *Gabbr1* RNAscope. For
635 the Imaris analysis, we compared the morphological complexity in two different ways.
636 First, we compared mCherry+ cells in control and mCherry+/Cas9-EGFP+ cells in cKO
637 (shown in **Figure 4f,g**). Second, we compared mCherry-/Cas9-EGFP+ cells and
638 mCherry+/Cas9-EGFP+ cells in cKO (shown in **Extended Data Fig 10d,e**). For EDNRB
639 or LHX2 expression and *Gabbr1* RNAscope, we compared mCherry+ cells in control

bioRxiv preprint doi: https://doi.org/10.1101/2023.03.14.532493; this version posted March 15, 2023. The copyright holder for this preprint (which was not certified by peer review) is the author/funder, who has granted bioRxiv a license to display the preprint in perpetuity. It is made available under aCC-BY-NC-ND 4.0 International license.

640 and mCherry+/Cas9-EGFP+ cells in cKO (shown in **Fig. 6k** and **Extended Data Fig**
641 **10b,c**). Above experiments were approved by Baylor College of Medicine IACUC.
642

643 **Immunofluorescence on frozen brain tissues**

644 Mice were anesthetized under isoflurane inhalation and perfused transcardially with
645 1XPBS pH 7.4 followed by 4% paraformaldehyde (PFA). Brains were removed, fixed in
646 4% PFA overnight, and placed in 20% sucrose for 24 hours before embedded in OCT.
647 Sections of 20 mm (morphological analysis using GFP labeling) were made on a
648 cryostat, washed with 1XPBS 5 min X2, incubated in antigen retrieval buffers at 75
649 degree 10 min, blocked with 10% goat or donkey serum in PBS with 0.3% Triton x-100,
650 and incubated with primary antibodies in blocking solution overnight. On the next day,
651 sections were incubated with secondary antibodies in PBS with 0.1% Triton x-100 for 1
652 h RT, followed by incubation with DAPI in PBS for 10min, and mounted with
653 VECTASHIELD Antifade Mounting Media (Vector Laboratories, H-1000). The following
654 primary antibodies were used: Chicken anti-GFP (1:1000; Abcam, ab13970), rabbit anti-
655 NFIA (1:500; Sigma, HPA006111), chicken anti-GFAP (1:1000; Abcam, ab4674),
656 mouse anti-GFAP (1:1000; EMD Millipore, MAB360), goat anti-SOX9 (1:750; RD
657 system, AF3075), rabbit anti-SOX9 (1:650; EMD Millipore, AB5535), rabbit anti-BRN2
658 (1:1000; Cell Signaling Technology, 12137S), rat anti-CTIP2 (1:500; Abcam, ab18465),
659 rabbit anti-FOXP2 (1:500; Abcam, ab16046), mouse anti-GAD67 (1:200; EMD Millipore,
660 MAB5406), mouse anti-Gephyrin (1:600; Synaptic Systems, 147011), rat anti-HA
661 (1:100; Sigma, 11867423001), rabbit anti-PSD95 (1:200; Thermo Fisher Scientific, 51-
662 6900), guinea pig anti-VGAT (1:350; Synaptic Systems, 131004), guinea pig anti-VGlut1

bioRxiv preprint doi: https://doi.org/10.1101/2023.03.14.532493; this version posted March 15, 2023. The copyright holder for this preprint (which was not certified by peer review) is the author/funder, who has granted bioRxiv a license to display the preprint in perpetuity. It is made available under aCC-BY-NC-ND 4.0 International license.

663 (1:2000; EMD Millipore, AB5905), guinea pig anti-VGlut2 (1:5000; EMD Millipore,
664 AB2251), rabbit anti-EDNRB (1:250, Abcam, ab117529), rabbit anti-LHX2 (1:250,
665 Abcam, ab184337), rabbit anti-NPAS3 (1:250; Thermo Fisher, PA5-20365). The
666 following secondary antibodies were used (1:500): Alexa Fluor 488 goat anti-chicken
667 (Thermo Fisher Scientific, A11039), Alexa Fluor 568 goat anti-rabbit (Thermo Fisher
668 Scientific, A11036), Alexa Fluor 568 donkey anti-goat (Thermo Fisher Scientific,
669 A11057), Alexa Fluor 568 goat anti-rat (Thermo Fisher Scientific, A11077), Alexa Fluor
670 488 goat anti-mouse (Thermo Fisher Scientiric, A32723), Alexa Fluor 647 goat anti-
671 guinea pig (Thermo Fisher Scientific, A21450).
672
673 **Confocal imaging and image analysis**
674 To evaluate astrocyte morphology, fluorescent images were acquired using a Zeiss
675 LSM 880 laser scanning confocal microscope with 63X oil immersion objective with
676 frame size at 1024 x 1024 and bit depth at 12 (Zen3.1) or a Leica TCS SP8 STED
677 microscope with 63X oil immersion objective with frame size at 1024 x 1024 (LAS X).
678 Serial images at z axis were taken at an optical step of 0.5 mm, with overall z axis range
679 encompassing the whole section. Images were imported to Imaris Bitplane software,
680 and only astrocytes with their soma between the z axis range were chosen for further
681 analysis[38]. We performed 3D surface rendering (**Fig. 1c-e,g-i, 2c,g-i, 4g-i, 6b,j-l,**
682 **Extended Data Fig. 1c,g, 3a-b,d,e, 8a-d, 10f,g)** using the Imaris Surface module, and
683 color coded the reconstructed surface images based on the surface area of each
684 astrocyte. Morphological analysis was performed using the Imaris Filament module.
685 Astrocyte branches and processes were outlined by Autopath with starting point set at 8

bioRxiv preprint doi: https://doi.org/10.1101/2023.03.14.532493; this version posted March 15, 2023. The copyright holder for this preprint (which was not certified by peer review) is the author/funder, who has granted bioRxiv a license to display the preprint in perpetuity. It is made available under aCC-BY-NC-ND 4.0 International license.

686 mm and seed point set at 0.7 mm, and statistical outputs including ‘‘filament number
687 Sholl intersections’’ were extracted and plotted with Prism software. Data were
688 generated from 3 brain sections per region per mouse with 3 mice per genotype. The
689 number of astrocytes analyzed were as follows: Gabbr1 control: OB 43, CX 27, HC 32,
690 BS 28, CB 29; Gabbr1 cKO: OB 31, CX 33, HC 30, BS 32, CB 29; Sox9 control: OB 29,
691 CX 35, HC 32, BS 36, CB 32; Sox9 cKO: OB 39, CX 33, HC 24, BS 24, CB 37; Nfia
692 control: OB 56, CX 52, HC 64, BS 28, CB 47; Nfia cKO: OB 60, CX 48, HC 65, BS 43,
693 CB 55; Interneuron Gq Saline: CX 49; Interneuron Gq CNO: CX 49; Interneuron Gi
694 Saline: CX 44; Interneuron Gi CNO: CX 71; CNO only: CX 39; P60 Interneuron Gq
695 Saline: CX 26; P60 Interneuron Gq CNO: 35; Gabbr1 Td control: CX 32, HC 30; Gabbr1
696 Td cKO: CX 36, HC 38; *sgEdnrb* control: CX 53: *sgEdnrb* cKO: CX 49; *sgLhx2* control:
697 CX 40; *sgLhx2* cKO: CX 42. To analyze number of astrocytes and knockout efficiency of
698 SOX9 and NFIA, fluorescent images were acquired using a Zeiss LSM 880 laser
699 scanning confocal microscope with 20X objective. Cell numbers were quantified by the
700 QuPath software Cell Detection function[39]. To measure the fluorescent intensity of
701 GFAP, fluorescent images were acquired using a Leica TCS SP8 STED microscope
702 with 20X objective or a Zeiss LSM 900 laser scanning confocal microscope with 40X oil
703 objective and were analyzed by Fiji. The person who analyzed the images was blinded
704 to the experimental groups.
705
706 **RNAscope**
707 Brain sections were acquired as described above and processed following the sample
708 preparation of fixed frozen tissues of RNAscope® Multiplex Fluorescent Reagent Kit v2

bioRxiv preprint doi: https://doi.org/10.1101/2023.03.14.532493; this version posted March 15, 2023. The copyright holder for this preprint (which was not certified by peer review) is the author/funder, who has granted bioRxiv a license to display the preprint in perpetuity. It is made available under aCC-BY-NC-ND 4.0 International license.

709 (Advanced Cell Diagnostics, 323100). The mouse *Gabbr1* probe was applied on brain
710 sections (Advanced Cell Diagnostics, 425181). After RNAscope incubation, the sections
711 were then immunostained for astrocyte markers as described above. The images were
712 acquired using a Leica TCS SP8 STED microscope with 63X oil immersion objective
713 with frame size at 1024 x 1024. Serial images at z axis were taken at an optical step of
714 0.5 mm, with overall z axis range encompassing the whole section. The quantification of
715 *Gabbr1* transcripts number and intensity were analyzed by Fiji.

716 **EdU cell proliferation assay**

717 P5 pups were Intraperitoneally injected with 100 mg/Kg EdU (Thermo Fisher Scientific,
718 C10337 or C10638) and collected at P7. Brain tissue was processed as described
719 above. After antigen retrieval, sections were washed with 10% goat serum in PBS for 5
720 minutes and applied Click-iT solution as described in the kit. After 30 minutes EdU
721 staining, sections were washed with 10% goat serum in PBS for 5 minutes, then
722 proceed to immunostaining with desired markers. Images were acquired using Zeiss
723 Axio Imager.M2 with apotome and 20X objective. To quantify proliferating astrocytes,
724 colocalization of EdU and astrocyte markers were analyzed by QuPath software.

725

726 **Slice recording**

727 Animals were deeply anesthetized with isoflurane. After decapitation, the brain was
728 quickly excised from the skull and submerged in an ice-cold cutting solution that
729 contained (in mM): 130 NaCl, 24 $NaHCO_3$, 1.25 NaH_2PO_4, 3.5 KCl, 1.5 $CaCl_2$, 1.5
730 $MgCl_2$, and 10 D(+)-glucose, pH 7.4. The whole solution was gassed with 95 % O2-5 %
731 CO_2. After trimming the hippocampal brain, 300 mm para-sagittal slices were cut using

bioRxiv preprint doi: https://doi.org/10.1101/2023.03.14.532493; this version posted March 15, 2023. The copyright holder for this preprint (which was not certified by peer review) is the author/funder, who has granted bioRxiv a license to display the preprint in perpetuity. It is made available under aCC-BY-NC-ND 4.0 International license.

732 a vibratome with a blade and transferred to extracellular ACSF solution (in mM): 130
733 NaCl, 24 $NaHCO_3$, 1.25 NaH_2PO_4, 3.5 KCl, 1.5 $CaCl_2$, 1.5 $MgCl_2$, and 10 D(+)-glucose,
734 pH 7.4. Slices were incubated at room temperature for at least one hour prior to
735 recording before being transferred to a recording chamber that was continuously
736 perfused with ASCF solution (flow rate = 2 ml/min) Slices were placed in a recording
737 chamber and target cells were identified via upright Olympus microscope with a 60X
738 water immersion objective with infrared differential interference contrast optics. Whole
739 cell recording was performed with□pCLAMP10 and□MultiClamp 700B amplifier (Axon
740 Instrument, Molecular Devices) at room temperature from layer II-III cortical neurons.
741 The holding potential was -60 mV. Pipette resistance was typically 5-8 MU. The pipette
742 was filled with an internal solution (in mM): 140 K-gluconate, 10 HEPES, 7 NaCl, and 2
743 MgATP adjusted to pH 7.4 with CsOH for action potential and passive conductance
744 measurements; 135 CsMeSO4, 8 NaCl, 10 HEPES, 0.25 EGTA, 1 Mg-ATP, 0.25 Na_2-
745 GTP, 30 QX-314, pH adjusted to 7.2 with CsOH (278-285 mOsmol) for EPSC
746 measurement; 135 CsCl, 4 NaCl, 0.5 $CaCl_2$, 10 HEPES, 5 EGTA, 2 Mg-ATP, 0.5 Na_2-
747 GTP, 30 QX-314, pH adjusted to 7.2 with CsOH (278-285 mOsmol) for IPSC
748 measurement. Spontaneous EPSCs were measured in the presence of $GABA_AR$
749 antagonist, bicuculline (20 µM, Tocris). IPSCs were measured in the presence of
750 ionotropic glutamate receptor antagonists, APV (50 µM, Tocris), and CNQX (20 µM,
751 Tocris). All holding potential values stated are after correction for the calculated junction
752 potential offset of 14 mV. Electrical signals were digitized and sampled at 50 µs
753 intervals with Digidata 1550B and Multiclamp 700B amplifier (Molecular Devices, CA,

bioRxiv preprint doi: https://doi.org/10.1101/2023.03.14.532493; this version posted March 15, 2023. The copyright holder for this preprint (which was not certified by peer review) is the author/funder, who has granted bioRxiv a license to display the preprint in perpetuity. It is made available under aCC-BY-NC-ND 4.0 International license.

754 USA) using pCLAMP 10.7 software. Data were filtered at 2 kHz. The recorded current
755 was analyzed with ClampFit 10.7 software.
756

757 **Two-photon GCaMP imaging in slices**

758 For two-photon imaging, mice were deeply anesthetized with isoflurane and then
759 perfused with cold artificial cerebrospinal fluid (ACSF, in mM:125 NaCl, 25 glucose, 25
760 $NaHCO_3$, 2.5 KCl, 2 $CaCl_2$, 1.25 NaH_2PO_4 and 1 $MgCl_2$, pH 7.3, 310–320 mOsm). The
761 brain was dissected and placed in an ice-cold ACSF. 300 mm thick brain slices were
762 sectioned on a vibratome. Slices were then recovered in oxygenated ACSF (37C) for 15
763 min and allowed to acclimate to room temperature for at least 15 min before imaging.
764 We recorded calcium traces using a two-photon resonant microscope (LSM 7MP, Zeiss)
765 equipped with a Coherent Chameleon Ultra (II) Ti-sapphire laser tuned to 900 nm and a
766 20x, 1.0 NA Zeiss objective. Calcium activity was typically sampled at ~1 Hz. Optical
767 signals were recorded for ~5 minutes per trial at 1024 x 1024 pixel resolution. We
768 recorded data from astrocytes at depths of ~30 mm below the surface. All multiphoton
769 imaging experiments were performed within 2-4 hours of slicing. For drug induced
770 calcium imaging, optical signals were recorded after slices were bathed in 500 nM
771 terodotoxin (TTX) for 5 minutes. After 2 minutes of recording under TTX treatment, brain
772 slices were bathed in 50 μM (R)-baclofen (Tocris, 0796) and recorded. Image analysis
773 of Ca^{2+} Spontaneous or drug-induced Ca^{2+} signal was detected in astrocytes expressing
774 GCaMP6s from the olfactory bulb or cortex. The detection of region of interest (ROI) for
775 soma and microdomain for Ca^{2+} imaging was performed in a semi-auto- mated manner
776 using the GECIquant program as described in a previous study[40]. After thresholding

bioRxiv preprint doi: https://doi.org/10.1101/2023.03.14.532493; this version posted March 15, 2023. The copyright holder for this preprint (which was not certified by peer review) is the author/funder, who has granted bioRxiv a license to display the preprint in perpetuity. It is made available under aCC-BY-NC-ND 4.0 International license.

777 from temporally projected stack images with a maximum intensity projection, a polygon
778 selection was manually drawn around the approximate astrocyte territory of interest,
779 and the selection was added to the ImageJ ROI manager. Note that the assignment of
780 territory was approximate and was not used for analysis. The area criterion was 20 mm^2
781 to infinity for soma within the GECIquant ROI detection function. Intensity values for
782 each ROI were extracted in ImageJ and converted to dF/F values. For each ROI, basal
783 F was determined during 40 s periods with no fluctuations. Clampfit 10.7 software was
784 used to detect and measure amplitude and frequency values for the somatic and
785 microdomain transients. We counted the response following with these criteria:
786 amplitude (> 0.5 dF/F), pre-trigger time (3 ms), and minimum duration (5 ms).
787

788 **Behavioral tests**

789 We subjected 3-month-old male mice to behavioral tests. All the experimental mice
790 were transferred to the testing room at least 30 min prior to the test. All tests were
791 performed with white noise at ± 60 dB in a designated room. The person performing the
792 tests was blinded to the experimental groups.
793

794 Three-chamber social interaction test: The three-chamber social interaction test was
795 performed in the arena having three chambers, left, middle and right chambers. On the
796 testing day, each animal was first habituated in the chambers with empty wire cages in
797 the left and right chamber for 10 minutes. After habituation, place either LEGO object or
798 partner mouse in the wire cages randomly. Total interaction time with partner mouse

bioRxiv preprint doi: https://doi.org/10.1101/2023.03.14.532493; this version posted March 15, 2023. The copyright holder for this preprint (which was not certified by peer review) is the author/funder, who has granted bioRxiv a license to display the preprint in perpetuity. It is made available under aCC-BY-NC-ND 4.0 International license.

799 was analyzed by ANY-maze software. All the partner mice were habituated to the wire
800 cages in the testing arena for 1 hour per day for 2 days before the day of testing.
801

802 Open field test: The open field tests were performed using the Versamax system. The
803 Versamax open field chamber is a square arena (40cm 3 40cm 3 30cm, Accuscan
804 Instruments) enclosed by transparent walls. Each mouse was put into the center of the
805 chamber. Locomotor activity was detected automatically by sensor beams at X, Y, and
806 Z directions. Data were recorded in 15 two-minute blocks for 30 min total and were
807 analyzed and exported with Versadat software.
808

809 Elevated plus maze: The elevated plus maze test were performed on a 1-meter high "+"
810 shaped apparatus with two open arms and two close arms. Mice were put into the
811 center of plus maze and recorded for 10 minutes. The time that mice spent on the open
812 arms or close arms were analyzed by ANYmaze software.
813

814 Prepulse inhibition: The prepulse inhibition test were performed using SR-LAB-Startle
815 Response System (San Diego Instrument). Mice were put into the cylinder tube in the
816 SR-LAB-Startle Response System chamber and habituated for 5 minutes. After 5
817 minutes habituation, mice were acclimated to a background white noise of 70 dB for
818 about 5 min prior to the prepulse inhibition test. Each test consisted of 48 trials
819 comprising of 6 blocks of eight trial types each presented in a pseudo random order.
820 Each block had a "No stimulus" trial used to measure baseline mouse response where
821 no sound was presented, a "acoustic startle response" trial comprised of a 40 ms, 120

bioRxiv preprint doi: https://doi.org/10.1101/2023.03.14.532493; this version posted March 15, 2023. The copyright holder for this preprint (which was not certified by peer review) is the author/funder, who has granted bioRxiv a license to display the preprint in perpetuity. It is made available under aCC-BY-NC-ND 4.0 International license.

822 dB sound burst, a "prepulse only" trials (74, 78 or 82 dB) comprising of three different 20
823 ms prepulses and finally the "prepulse inhibition (PPI)" trials composed of the
824 presentation of one of the three prepulse sounds, 100 ms prior to the 120 dB startle
825 stimulus. The inter-trial interval ranged from 10 s to 20 s, and the startle response was
826 recorded every 1 ms for 65 ms following the onset of the startle stimulus. Percent PPI of
827 the startle response was calculated as follows: 100 – [(response to acoustic prepulse
828 plus startle stimulus trials/startle response alone trials) × 100].
829
830 Parallel rod footfall test: The parallel rod foot slip test was performed in a chamber with
831 metal grid floor. For 10 minutes recording, mice freely moved in the chamber. When
832 mice foot slipped on the floor, the ANY-maze software counted as one footfall. The
833 recorded data were analyzed by ANY-maze software.
834
835 Rotarod: The rotarod test were performed on a rotating rod. It's a 2-day protocol
836 consisting of 4 trials per day. Each trial lasted for 5 minutes with the rod accelerating at
837 a speed of 4–40 rpm in 5 minutes. The time spent walking on the rod was recorded.
838 Intertrial interval was at least 10–15 minutes.
839
840 Contextual/cued conditional fear: The contextual conditional fear test was performed in
841 a chamber with metal grid floor. Three checkerboard pattern visual cues (13 cm X 13
842 cm) were posted at three sides of the chamber. On day 1, mice were put into the center
843 of the chamber and allowed to move freely for 3 min before being exposed to 3 mild foot
844 shocks (2 s, 0.7mA) with 2 min intertrial intervals (ITI) between each shock (figure). On

bioRxiv preprint doi: https://doi.org/10.1101/2023.03.14.532493; this version posted March 15, 2023. The copyright holder for this preprint (which was not certified by peer review) is the author/funder, who has granted bioRxiv a license to display the preprint in perpetuity. It is made available under aCC-BY-NC-ND 4.0 International license.

845 day 2, mice were first put back to the same chamber and movements of mice over 5
846 min were recorded and analyzed by FreezeFrame software (Actimetrics, Coulbourn
847 Instruments) with the bouts and threshold both set at 6.0 s. % freezing time identified
848 based on the above criteria. Two hours after contextual conditional fear, mice were put
849 back to chamber with different context and were recorded % freezing time upon cue
850 stimulation. The % freezing time in cued conational fear was analyzed by same criteria
851 as contextual conditional fear. Data were then plotted as shown in Figure.
852
853 **FACS sorting**
854 We harvested different regions from mouse brains and dissociated them using the
855 protocol described previously[14]. Dissociated astrocytes from different regions were
856 gated with BD FACSDiva Software and sorted by BD FACSAira III with 100 mM nozzle.
857 Around 95,000 GFP^+ astrocytes were collected per 1.5 mL tube, which contained 650 µl
858 of Buffer RLT (QIAGEN Cat. No. 79216) with 1% b-Mercaptoethanol. Finally, each
859 sample was vortexed and rapidly frozen on dry ice.
860
861 **Tissue dissociation for single cell sequencing**
862 Brain slices were prepared as we described in slicing recording methods. The desired
863 brain region was micro-dissected in ACSF on ice, followed by tissue dissociation using
864 neural tissue dissociation kit (Miltenyi Biotec). After 30 minutes incubation on
865 gentleMACS (Miltenyi Biotec), samples were treated with debris removal kit, 1X red
866 blood cell lysis buffer, dead cell removal kit (Miltenyi Biotec) to purify single cells. To

bioRxiv preprint doi: https://doi.org/10.1101/2023.03.14.532493; this version posted March 15, 2023. The copyright holder for this preprint (which was not certified by peer review) is the author/funder, who has granted bioRxiv a license to display the preprint in perpetuity. It is made available under aCC-BY-NC-ND 4.0 International license.

867 remove microglia in samples, CD11b microbeads were applied. Finally, samples were
868 subject to single cell RNA-sequencing library preparation.
869
870 **RNA extraction, library preparation and sequencing**
871 For the whole transcriptomic RNA-sequencing, RNA was extracted from pelleted cells
872 using RNeasy Micro Kit (Cat. No. 74004, QIAGEN). RNA integrity (RIN R 8.0) was
873 confirmed using the High Sensitivity RNA Analysis Kit (DNF-472-0500, Agilent formerly
874 AATI) on a 12-Capillary Fragment Analyzer. cDNA synthesis and Illumina sequencing
875 libraries with 8-bp single indices were constructed from 10 ng total RNA using the Trio
876 RNASeq System (0507-96, NuGEN). The resulting libraries were validated using the
877 Standard Sensitivity NGS Fragment Analysis Kit (DNF-473-0500, Agilent formerly AATI)
878 on a 12-Capillary Fragment Analyzer and quantified using Quant-it dsDNA assay kit
879 (Cat. Q33120). Equal concentrations (2 nM) of libraries were pooled and subjected to
880 paired-end (R1: 75, R2: 75) sequencing of approximately 40 million reads per sample
881 using the High Output v2 kit (FC-404-2002, Illumina) on a NextSeq550 following the
882 manufacturer's instructions. For single-cell RNA-sequencing, single cell gene
883 expression library was prepared according to Chromium Single Cell Gene Expression
884 3v3.1 kit (10x Genomics). In Brief, single cells, reverse transcription (RT) reagents, Gel
885 Beads containing barcoded oligonucleotides, and oil were loaded on a Chromium
886 controller (10x Genomics) to generate single cell GEMS (Gel Beads-In-Emulsions)
887 where full length cDNA was synthesized and barcoded for each single cell.
888 Subsequently the GEMS are broken and cDNA from each single cell are pooled.
889 Following cleanup using Dynabeads MyOne Silane Beads, cDNA is amplified by PCR.

bioRxiv preprint doi: https://doi.org/10.1101/2023.03.14.532493; this version posted March 15, 2023. The copyright holder for this preprint (which was not certified by peer review) is the author/funder, who has granted bioRxiv a license to display the preprint in perpetuity. It is made available under aCC-BY-NC-ND 4.0 International license.

890 The amplified product is fragmented to optimal size before end-repair, A-tailing, and
891 adaptor ligation. Final library was generated by amplification. Equal concentrations (2
892 nM) of libraries were pooled and subjected to paired-end (R1: 26, R2: 50) sequencing
893 using the High Output v2 kit (FC-404-2002, Illumina) on a NextSeq550 following the
894 manufacturer's instructions.
895
896 **RNA-Seq bioinformatics analysis**
897 Sequencing files from each flow cell lane were downloaded and the resulting fastq files
898 were merged. Quality control was performed using fastQC (v0.10.1) and MultiQC
899 (v0.9)[41]. Reads were mapped to the mouse genome mm10 assembly using STAR
900 (v2.5.0a)[42]. RNA-seq analysis were analyzed and plotted as previously described[26].
901 RNA-Seq data can be found at the NIH GEO database (GSE198632).
902
903 **Single cell RNA-seq analysis**
904 Sequencing files from each flow cell lane were downloaded and the resulting fastq files
905 were merged. Reads were mapped to the mouse genome mm10 assembly using 10X
906 Cell Ranger (3.0.2) and it is estimated 15,000-38,000 mean reads per cell. For single
907 cell sequencing analysis, standard procedures for filtering, mitochondrial gene removal,
908 doublets removal, variable gene selection, dimensionality reduction, and clustering were
909 performed using Seurat (version 4.1.0) and DoubletFinder[21,43]. Criteria for cell inclusion
910 were minimum nUMI/cell threshold 200, minimum gene/cell threshold 250, minimum
911 log10gene/UMI threshold 0.8, maximum mitochondria ratio 0.3, and minimum ribosome
912 ration 0.01[44]. Mitochondrial genes were removed before doublets removal. Principle

bioRxiv preprint doi: https://doi.org/10.1101/2023.03.14.532493; this version posted March 15, 2023. The copyright holder for this preprint (which was not certified by peer review) is the author/funder, who has granted bioRxiv a license to display the preprint in perpetuity. It is made available under aCC-BY-NC-ND 4.0 International license.

913 component analysis and elbowplot were used to find neighbors and clusters (resolution
914 0.3). Cells were visualized using a 2-dimensional Uniform Manifold Approximation and
915 Projection (UMAP) of the PCprojected data. Molecularly distinct cell populations were
916 assigned to each cluster using singleR with adult mouse cortical cell taxonomy single
917 cell RNA-seq data as references[45,46]. FindAllMarkers were used to identify all
918 differentially expressed markers between clusters. Annotated clusters were refined
919 based on those unique markers. Differentially expressed genes (DEGs) in neurons
920 between Gabbr1 control and cKO were identified by identified by FindMarkers using
921 default settings. 2021 KEGG mouse pathway analysis of DEGs were performed using
922 enrichR[47]. Single cell RNA-Seq data can be found at the NIH GEO database
923 (GSE198357, GSE198633).
924

925 **Inference and analysis of cell–cell communication**

926 Cell-cell communications between astrocytes and neurons were inferred using CellChat
927 algorithm[22]. We followed the CellChat workflow, and first identified cell type specific
928 communication within Gabbr1cKO and control experiments separately. Next, we used
929 CellChat to compare the total number of interactions and interaction strength of the
930 inferred cell-cell communication networks in Gabbr1cKO and control experiments. We
931 used netVisual_diffInteraction function to visualize differential number of interactions or
932 interaction strength among Gabbr1cKO and control conditions. Finally, we identified the
933 upgulated and down-regulated signaling ligand-receptor pairs in Gabbr1cKO compared
934 to the control dataset using netVisual_bubble function.
935

bioRxiv preprint doi: https://doi.org/10.1101/2023.03.14.532493; this version posted March 15, 2023. The copyright holder for this preprint (which was not certified by peer review) is the author/funder, who has granted bioRxiv a license to display the preprint in perpetuity. It is made available under aCC-BY-NC-ND 4.0 International license.

936 **Co-immunoprecipitation and western Blot**

937 Animal tissues were dissected, washed with cold PBS three times, and dissociated
938 using a pellet homogenizer. RIPA lysis buffer (50 mM Tris-HCl pH 7.5, 150 mM NaCl,
939 0.5% sodium deoxycholate, 0.1% SDS, 1% NP-40) was used for preparing input control
940 lysates. For co-IP, nuclear lysates were prepared using NE-PER Nuclear and
941 Cytoplasmic Extraction Reagents (ThermoFisher, 78833) according to the
942 manufacturer's instructions. Brain tissues from 6-8 animals were pulled together to have
943 enough nuclear lysates for each IP. 3mg of nuclear lysates were used for IP with 2 μg
944 IgG or 5 μg primary antibodies (normal mouse IgG, Santa Cruz Biotechnology, sc-2025;
945 normal rabbit IgG, R&D Systems, AB-105-C; mouse anti-LHX2, Santa Cruz
946 Biotechnology, sc-81311; rabbit anti-SOX9, EMDMillipore, ab5535) for overnight at 4
947 °C. Protein A agarose beads (ThermoFisher, 15918-014) was added for subsequent
948 pull-down for an additional 4 h at 4 °C. The beads were collected, washed, and boiled in
949 2× SDS gel loading dye to elute immunoprecipitated proteins for Western blot analysis.
950 Input control lysates (20 ug) and immunoprecipitated proteins were run on a 8% SDS
951 polyacrylamide gel, followed by transferring onto nitrocellulose membrane at 350 mA for
952 65 min. 5% milk in Tris-buffered saline with Tween20 (TBST) was used to block the
953 membrane, followed by incubating primary antibodies at 1:1,000 dilution (rabbit anti-
954 LHX2, Abcam, ab184377; rabbit anti-NFIA, Sigma, HPA006111; rabbit anti-SOX9,
955 EMDMillipore, ab5535; rabbit anti-NPAS3, ThermoFisher, PA520365) for overnight at 4
956 °C. The next day, membranes were washed three times with TBST, incubated with
957 horseradish peroxidase-conjugated anti-rabbit or anti-mouse IgG at 1:2,000 dilution in
958 5% milk in TBST at room temperature for 1 h. Membranes were then washed with TBST

bioRxiv preprint doi: https://doi.org/10.1101/2023.03.14.532493; this version posted March 15, 2023. The copyright holder for this preprint (which was not certified by peer review) is the author/funder, who has granted bioRxiv a license to display the preprint in perpetuity. It is made available under aCC-BY-NC-ND 4.0 International license.

959 three times before developing with luminol reagent (Santa Cruz Biotechnology, sc-
960 2048).
961

962 **Chromatin immunoprecipitation PCR (ChIP-PCR)**

963 Mouse cortex and olfactory bulbs were collected for ChIP experiments. Dissociated
964 cortexes or olfactory bulbs were pooled together from 2-3 animals for each ChIP
965 experiment. Chromatin was crosslinked by using freshly prepared 1.1% formaldehyde
966 solution with rocking at room temperature for 10 min, followed by addition of 0.1 M
967 glycine. Cell pellets were collected by centrifugation at 3500 rpm for 5 min at 4 C,
968 washed with PBS and frozen at 80 C or used immediately for preparing lysates. Pellets
969 were resuspended with PBS/PMSF containing 0.5% Igepal to release nuclei, followed
970 by washing with cold ChIP-Buffer (0.25% TritonX, 10 mM EDTA, 0.5 mM EGTA, 10 mM
971 HEPES pH 6.5) and nuclei were lysed with ChIP lysis buffer (0.5% SDS, 5 mM EDTA,
972 25 mM Tris-HCl pH 8) for 15-20 min at room temperature. Lysates were sonicated to
973 250-350 bp using Diagenode Bioruptor. Immunoprecipitation was carried out by rotating
974 sonicated lysates overnight at 4 C with NFIA antibody (5 mg, Sigma, HPA006111) or
975 SOX9 antibody (EMD Millipore, AB5535) followed by pull-down using Protein A/G
976 agarose beads (Thermo Fisher Scientific, 15918014) for 6 hours. The beads were
977 collected and washed with TSE1 buffer (0.1% SDS, 1% TritonX, 2 mM EDTA, 20 mM
978 Tris-HCl pH 8, 150 mM NaCl), TSE2 buffer (TSE1 buffer with 500 mM NaCl), LiCl buffer
979 (0.25M lithium chloride, 1% NP40, 1% sodium deoxycholate, 1 mM EDTA, 10 mM Tris-
980 HCl pH 8) and TE buffer. Immunoprecipitated chromatin was then eluted by heating the
981 beads in ChIP Elution buffer (1% SDS, 0.1 M $NaHCO_3$) at 65 C for 20 min twice. A

bioRxiv preprint doi: https://doi.org/10.1101/2023.03.14.532493; this version posted March 15, 2023. The copyright holder for this preprint (which was not certified by peer review) is the author/funder, who has granted bioRxiv a license to display the preprint in perpetuity. It is made available under aCC-BY-NC-ND 4.0 International license.

982 small sample of elution was used for Western Blot analysis to confirm
983 immunoprecipitation of NFIA. ChIP-DNA was quantified using Quant-it dsDNA assay kit
984 (Cat. Q33120) and used for ChIP-PCR. Primers for NFIA binding motif and SOX9 on
985 Gabbr1 promoter: Forward 5'- TTCAAGGTCTGTTCCCCAGGC -3', Reverse 5'-
986 GAGGGCGTAGAGGTAGGATGGA -3'.
987

988 **Intraventricular injection of AAV viruses**

989 For interneuron hM3Dq experiments, we used AAV2/9-pAAV-hDlx-hM3Dq-dTomato-
990 Fishell-4 (Addgene, 83897) and AAV2/9-pAAV-hDlx-hM4Di-dTomato-Fishell-5
991 (Addgene, 83896) at a concentration of 6+13 genome copies per ml (gc/ml). For the
992 GCaMP experiments in *Sox9* olfactory bulb experiments, we generated pAAV-GFAP-
993 GCaMP6m plasmid from flexed-GCaMP6 and pZac2.1-GfaABC1D-mCherry-
994 hPMCA2w/b (Addgene, 111568) and used AAV2/9-pAAV-GFAPGCaMP6m at a
995 concentration of 1.07527E+13 genome copies per ml (gc/ml). For interneuron labeling
996 experiments, we generated pAAV-mDlxRuby2 plasmid from pAAV-mDlx-NLS-Ruby2
997 (Addgene, 99130) and used AAV2/9-pAAV-mDlx-Ruby2 at a concentration of
998 2.344E+13 genome copies per ml (gc/ml)[48]. For intraventricular injection, P1 pups were
999 anesthetized with hypothermia and injected AAV virus as described in previous paper[49].
1000 2.5 µl of Trypan Blue (Thermo Fisher Scientific, 15250061) was mixed with 10 µl of
1001 virus before injection. AAV virus: All AAV viruses were generated by the Optogenetics
1002 and Viral Vectors Core at Jan and Dan Duncan Neurological Research Institute (NRI).
1003 For astrocyte, CRISPR-dependent tissue specific knockout experiments, we utilized
1004 pZac2.1-U6-sgRNA empty-GfaABC1D-mcherry (Khakh lab) to generate pAAV-U6-

bioRxiv preprint doi: https://doi.org/10.1101/2023.03.14.532493; this version posted March 15, 2023. The copyright holder for this preprint (which was not certified by peer review) is the author/funder, who has granted bioRxiv a license to display the preprint in perpetuity. It is made available under aCC-BY-NC-ND 4.0 International license.

1005 Ednrb sgRNA-Gfap-mcherry and pAAV-U6-Lhx2 sgRNA-Gfap-mcherry by amplifying
1006 sgRNA inserts with forward primers: CACCGTCAATATTTCGTTGGCACGG (*Ednrb*),
1007 CACCGGCTGCACAGAGAACCGCCTG (*Lhx2*) and reverser primers:
1008 AAACCCGTGCCAACGAAATATTGAC (*Ednrb*),
1009 AAACCAGGCGGTTCTCTGTGCAGCC (*Lhx2*). We used AAV2/9-pAAV-Gfap-Cre-P2A-
1010 TurboRFP at a concentration of 5E+12 genome copies per ml (gc/ml) and AAV2/9-
1011 pAAV-U6-Ednrb sgRNA-Gfap-mcherry or AAV2/9-pAAV-U6-Lhx2 sgRNA-Gfap-mcherry
1012 at a concentration of 2E+12 genome copies per ml (gc/ml). All animal procedures were
1013 done in accordance with approved BCM IACUC protocols.

1014 **QUANTIFICATION AND STATISTICAL ANALYSIS**

1015 Sample sizes and statistical tests can be found in accompanying Figure legends. Offline
1016 analysis was carried out using Clampfit 10.7, Minianalysis, SigmaPlot 13, Prism 9, and
1017 Excel software. we do not assume that our data are normally distributed and perform
1018 either linear or generalized mixed-effects model for repeated measurements. If the
1019 number of paired animals is more than 3, we used Mann-Whitney test based on the
1020 number of animals. For the number of paired animal equals to 3, we used either linear
1021 or generalized linear mixed-effects model (LME or GLME) to consider the variances
1022 from both cells and animals. We chose between LME or GLME based on the data
1023 distribution. We used Shapiro-Wilk test to test whether the analyzed cells are normally
1024 distributed. If the data is normally distributed, we used LME to perform statistical
1025 analysis. If the data is not normally distributed, we used GLME to analyze the data.
1026 Data are presented as mean ± SEM (standard error of the mean). Levels of statistical

bioRxiv preprint doi: https://doi.org/10.1101/2023.03.14.532493; this version posted March 15, 2023. The copyright holder for this preprint (which was not certified by peer review) is the author/funder, who has granted bioRxiv a license to display the preprint in perpetuity. It is made available under aCC-BY-NC-ND 4.0 International license.

1027 significance are indicated as follows: * ($p < 0.05$), ** ($p < 0.01$), *** ($p < 0.001$), **** ($p <$
1028 0.0001).
1029
1030
1031 **Reporting summary**

1032 Further information on research design is available in the Nature Research Reporting
1033 Summary linked to this paper.
1034

1035 **Data availability**

1036 The bulk RNA-seq data from developing astrocytes and Ednrb1-cKO astrocytes has
1037 been deposited in the NCBI Gene Expression Omnibus (GEO) under accession number
1038 GSE198632. Single cell RNA-Seq data can be found at the NIH GEO database
1039 (GSE198357, GSE198633). All other data in this article are available from the
1040 corresponding author upon reasonable request.
1041

1042 **Code availability**

1043 No custom code was used. R package limma eBayes function was used to define
1044 differentially expressed genes. Bioconductor SVA/Combat package was used for batch
1045 correction.
1046
1047
1048
1049
1050
1051 **References**

1052

bioRxiv preprint doi: https://doi.org/10.1101/2023.03.14.532493; this version posted March 15, 2023. The copyright holder for this preprint (which was not certified by peer review) is the author/funder, who has granted bioRxiv a license to display the preprint in perpetuity. It is made available under aCC-BY-NC-ND 4.0 International license.

1053 36. Haller, C. *et al.* Floxed allele for conditional inactivation of the GABA B(1)gene.
1054 *genesis* 40, 125–130 (2004).

1055 37. Akiyama, H., Chaboissier, M.-C., Martin, J. F., Schedl, A. & Crombrugghe, B. de.
1056 The transcription factor Sox9 has essential roles in successive steps of the chondrocyte
1057 differentiation pathway and is required for expression of Sox5 and Sox6. *Gene Dev* 16,
1058 2813–2828 (2002).

1059 38. Lanjakornsiripan, D. *et al.* Layer-specific morphological and molecular differences in
1060 neocortical astrocytes and their dependence on neuronal layers. *Nature*
1061 *Communications* 9, 1–15 (2018).

1062 39. Bankhead, P. *et al.* QuPath: Open source software for digital pathology image
1063 analysis. *Sci Rep-uk* 7, 16878 (2017).

1064 40. Srinivasan, R. *et al.* Ca2+ signaling in astrocytes from Ip3r2–/– mice in brain slices
1065 and during startle responses in vivo. *Nat Neurosci* 18, 708–717 (2015).

1066 41. Ewels, P., Magnusson, M., Lundin, S. & Käller, M. MultiQC: summarize analysis
1067 results for multiple tools and samples in a single report. *Bioinformatics* 32, 3047–3048
1068 (2016).

1069 42. Dobin, A. *et al.* STAR: ultrafast universal RNA-seq aligner. *Bioinformatics* 29, 15–21
1070 (2013).

1071 43. McGinnis, C. S., Murrow, L. M. & Gartner, Z. J. DoubletFinder: Doublet Detection in
1072 Single-Cell RNA Sequencing Data Using Artificial Nearest Neighbors. *Cell Syst* 8, 329-
1073 337.e4 (2019).

1074 44. Ximerakis, M. *et al.* Single-cell transcriptomic profiling of the aging mouse brain. *Nat*
1075 *Neurosci* 22, 1696–1708 (2019).

1076 45. Aran, D. *et al.* Reference-based analysis of lung single-cell sequencing reveals a
1077 transitional profibrotic macrophage. *Nat Immunol* 20, 163–172 (2019).

1078 46. Tasic, B. *et al.* Adult mouse cortical cell taxonomy revealed by single cell
1079 transcriptomics. *Nat Neurosci* 19, 335–346 (2016).

1080 47. Kuleshov, M. V. *et al.* Enrichr: a comprehensive gene set enrichment analysis web
1081 server 2016 update. *Nucleic Acids Res* 44, W90–W97 (2016).

1082 48. Chen, T.-W. *et al.* Ultrasensitive fluorescent proteins for imaging neuronal activity.
1083 *Nature* 499, 295–300 (2013).

bioRxiv preprint doi: https://doi.org/10.1101/2023.03.14.532493; this version posted March 15, 2023. The copyright holder for this preprint (which was not certified by peer review) is the author/funder, who has granted bioRxiv a license to display the preprint in perpetuity. It is made available under aCC-BY-NC-ND 4.0 International license.

1084 49. Kim, J.-Y., Grunke, S. D., Levites, Y., Golde, T. E. & Jankowsky, J. L.
1085 Intracerebroventricular Viral Injection of the Neonatal Mouse Brain for Persistent and
1086 Widespread Neuronal Transduction. *J Vis Exp* 51863 (2014) doi:10.3791/51863.

1087

1088

1089

1090

1091 Extended Data Figure Legends

1092

1093 **Extended Data Figure 1. Normalization of astrocyte morphology in the adult after**
1094 **developmental activation of inhibitory neurons**

1095 **a-b.** Analysis of SOX9 (e) and Ki67(f) expression within Aldh1l1-GFP astrocytes at P21
1096 after activation of inhibitory neurons (or control); quantification was derived from $n = 3$
1097 pairs of animals (**a**, 20,24 images; GLME; **b**, 12, 11 images; GLME). **c.** CNO only
1098 treatment of Aldh1l1-GFP mice from P7-P21 and analysis of astrocyte morphology at
1099 P21. $n = 3$ animals (39 cells; GLME model with Sidak's multiple comparisons test). **d.**
1100 Heatmap depicting expression of GABA receptor subunits in developing astrocytes from
1101 the cortex (CX), hippocampus (HC), or olfactory bulb (OB) at P1, P7, and P14. See
1102 Extended Data Figure 2. **d.** Example of gating strategy and percentage of GFP^+
1103 astrocytes FACS isolated from P1 animal. **e.** Heatmap depicting expression of GABA
1104 receptor subunits in developing astrocytes from the cortex (CX), hippocampus (HC), or
1105 olfactory bulb (OB) at P1, P7, and P14. See Extended Data Figure 2. **f.** Schematic of
1106 DREADD-based activation of inhibitory neurons in post-natal Aldh1l1-GFP mice and
1107 experimental timeline. **g.** Imaging of P60 Aldh1l1-GFP astrocytes after hM3Dq

bioRxiv preprint doi: https://doi.org/10.1101/2023.03.14.532493; this version posted March 15, 2023. The copyright holder for this preprint (which was not certified by peer review) is the author/funder, who has granted bioRxiv a license to display the preprint in perpetuity. It is made available under aCC-BY-NC-ND 4.0 International license.

1108 activation of inhibitory neurons; quantification of morphological complexity using Scholl
1109 analysis, branch number, and total processes at P21; *n* = 3 pairs of animals (26,35
1110 cells; upper, GLME model with Sidak's multiple comparisons test; bottom, GLME
1111 model). Scale bars, 20 µm (**a-c**), 30 µm (**g**). Data represent mean ± s.d. (**a-c**, **g** upper),
1112 median, minimum value, maximum value and IQR (**g** bottom).

1113

1114 **Extended Data Figure 2. Transcriptomic RNA-Sequencing analysis of developing**
1115 **astrocytes in the cortex, hippocampus, and olfactory bulb at P1, P7, and P14.**

1116 **a.** Heatmap depicting the expression of neuron-specific and astrocyte-specific genes
1117 from P1, P7, and P14 FACS isolated Aldh1l1-GFP astrocytes from the listed brain
1118 regions. **b.** Aldh1l1-GFP astrocytes from the cortex at P1, P7, P14. Principal component
1119 (PC) analysis against top 2,000 variable genes across the region and timepoints
1120 examined from 3-4 animals in each group. **c.** Heatmap depicting differential patterns of
1121 gene expression in developing astrocytes across brain regions and timepoints. **d**. Gene
1122 Ontology (GO) analysis of the common and region-specific patterns of gene expression.
1123 **e-f.** *Ald1l1-CreER; ROSA-LSL-tdTomato* mouse line treated with tamoxifen at P1,
1124 harvested at P28. Co-immunostaining of tdTomato labeled cells with Sox9, Olig2,
1125 NeuN, and Iba1 demonstrating astrocyte-specific activity of Aldh1l1-CreER line. *n* = 4
1126 animals. Scale bars, 10 µm (**b**), 40 µm (**e-h**).

1127

1128 **Extended Data Figure 3. Analysis of astrocyte development in the *Gabbr1-cKO***
1129 **mouse line.**

bioRxiv preprint doi: https://doi.org/10.1101/2023.03.14.532493; this version posted March 15, 2023. The copyright holder for this preprint (which was not certified by peer review) is the author/funder, who has granted bioRxiv a license to display the preprint in perpetuity. It is made available under aCC-BY-NC-ND 4.0 International license.

1130 **a.** Imaging of Aldh1l1-GFP astrocytes from the brain stem and cerebellum at P28;
1131 quantification of morphological complexity was derived from $n = 3$ pairs of animals
1132 (*Gabbr1 control*: BS 28, CB 29; *Gabbr1 cKO*: BS 32, CB 29 cells; GLME model with
1133 Sidak's multiple comparisons test, $^{*}P = 0.0179$, 0.0167). **b.** Quantitative analysis of
1134 branch points and process length from all brain regions analyzed; $n = 25$-38 cells from 3
1135 pairs of animals (*Gabbr1 control*: OB 38, CX 30, HC 29, BS 28, CB 25; *Gabbr1 cKO*:
1136 OB 33, CX 30, HC 29, BS 32, CB 29 cells; two way ANOVA, $^{**}P = 0.0014$, $^{*}P = 0.0174$,
1137 $P = 0.9040$, $^{*}P = 0.0132$, $P = 0.7126$, $^{**}P = 0.0054$, $^{****}P < 0.0001$, $^{**}P = 0.0066$, $P =$
1138 0.3763). **c.** Schematic describing the experimental timeline and mouse lines rendering
1139 astrocyte-specific knockout of *Gabbr1* for sparse labeling experiments. **d-e**. Imaging
1140 and quantification of sparsely labeled, tdTomato-expressing astrocytes from *Gabbr1-*
1141 *cKO* and *control* mice from the cortex (d) and hippocampus (e); $n = 3$ pairs of animals
1142 (*Gabbr1 control*: CX 32, HC 30; *Gabbr1 cKO*: CX 36, HC 38 cells; **d,e** upper, GLME
1143 model with Sidak's multiple comparisons test, $^{*}P = 0.0213$, $^{**}P = 0.0012$; **d,e** bottom,
1144 GLME model, $^{***}P = 0.00043$, $^{**}P = 0.0027$, $^{***}P = 0.00042$, $^{****}P<0.0001$). **f.** Antibody
1145 staining for SOX9 in Aldh1l1-GFP astrocytes from cortex of *Gabbr1-cKO* and control;
1146 quantification is derived from $n = 3$ pairs of animals (35 images; GLME model). **g.**
1147 Pulse-chase EdU-labeling and antibody staining at P28 from all brain regions analyzed;
1148 quantification is derived from $n = 3$ pairs of animals (*Gabbr1 control*: OB 9, CX 9, HC 9,
1149 BS 9, CB 9; *Gabbr1 cKO*: OB 8, CX 9, HC 9, BS 9, CB 9 images; GLME model). Scale
1150 bars, 30 μm (**a**), 20 μm (**d-g**). Data represent mean ± s.d. (**a-b**, **d-e** upper, **f-g**), median,
1151 minimum value, maximum value and IQR (**d-e** bottom).
1152

bioRxiv preprint doi: https://doi.org/10.1101/2023.03.14.532493; this version posted March 15, 2023. The copyright holder for this preprint (which was not certified by peer review) is the author/funder, who has granted bioRxiv a license to display the preprint in perpetuity. It is made available under aCC-BY-NC-ND 4.0 International license.

1153 **Extended Data Figure 4. RNA-Seq of *Gabbr1-cKO* astrocytes and single cell RNA-**
1154 **Seq analysis of *Gabbr1-cKO* cortex.**
1155 **a.** Serut analysis of single cell RNA-Seq (scRNA-Seq) from *Gabbr1-cKO* and controls
1156 from P28 cortex. **b.** Quantification of cell clusters identifying CNS cell types from
1157 scRNA-Seq data. **c-e**. Dot plot summaries demonstrating CellChat interaction profiles
1158 and expression patterns of key astrocyte-neuron interaction pathways.
1159

1160 **Extended Data Figure 5. Analysis of cortical neurons in the *Gabbr1-cKO* mouse**
1161 **line and behavioral studies.**
1162 **a.** Antibody staining for BRN2 (Layers II/II). **b.** CTIP2 (Layers V). **c.** FOXP2 (Layers VI)
1163 layer-specific neuronal markers in the P28 cortex from *Gabbr1-cKO* and *control*;
1164 quantification is derived from n = 11-12 images from 3 pairs of animals (*control* 12, *cKO*
1165 11 images; GLME model). **d.** Schematic of synaptic markers and cortical layers. **e-f.**
1166 Antibody staining for makers of excitatory synapses Vglut1/PSD95 (e) and
1167 Vglut2/PSD95 (f) in layer I of the cortex from *Gabbr1-cKO* or *control* mice at P28 (n =3
1168 pairs of animals; GLME model, *P = 0.0490). **g.** Antibody staining for markers of
1169 inhibitory synapses VGAT/Gephyrin at P28; quantification is derived from 3 pairs of
1170 animals (GLME model). **h-m**. Summary of behavioral assays conducted on Gabbr1-
1171 cKO and control animals including open field (h), elevated plus maze (i), rotarod (j),
1172 parallel foot fall (k), contextual fear conditioning (l), and cued fear conditioning (m).; data
1173 is derived from 10 *control* and 11 *Gabbr1-cKO* animals (two-tailed Mann-Whitney test,
1174 ***P = 0.0004). Scale bars, 100 μm (**a-c**), 3 μm (**e-g**). Data represent mean ± s.d. (**a-c**,
1175 **e-m**).

bioRxiv preprint doi: https://doi.org/10.1101/2023.03.14.532493; this version posted March 15, 2023. The copyright holder for this preprint (which was not certified by peer review) is the author/funder, who has granted bioRxiv a license to display the preprint in perpetuity. It is made available under aCC-BY-NC-ND 4.0 International license.

1176

1177 **Extended Data Figure 6. Electrophysiological recordings from cortical excitatory**
1178 **neurons from *Gabbr1-cKO***

1179 **a.** Two-photon, slice imaging of GCaMP6s activity in *control* and *Gabbr1-cKO*
1180 astrocytes from the cortex at P28. Quantification of Ca^{2+} activity in astrocytic
1181 microdomains in the *Gabbr1-cKO* and *control* animals, quantification is derived from n =
1182 3 pairs of animals (19, 30 cells; GLME model). **b-e.** Representative traces of action
1183 potential in layer II/III excitatory neurons upon varying injected current in *Gabbr1-cKO*
1184 and *control* (b). Summary data of action potential firing (c; two way ANOVA). Summary
1185 data of resting membrane potential (d; two-tailed unpaired Welch's t-test) and threshold
1186 (e; two-tailed unpaired Welch's t-test) from 3 pairs of animals (n = 13, 12 cells). **f-i.**
1187 Representative traces of action potential in layer II/III inhibitory neurons upon varying
1188 injected current in *Gabbr1-cKO* and *control* (f). Summary data of action potential firing
1189 (g; two way ANOWA). Summary data of resting membrane potential (h; two-tailed
1190 unpaired Welch's t-test, $^{**}P = 0.0091$) and threshold (i; two-tailed unpaired Welch's t-
1191 test) from 3 pairs of animals (n = 12, 15 cells). Scale bars, 20 μm (**a**). Data represent
1192 median, minimum value, maximum value and IQR (**a**), mean ± s.e.m. (**c-e**, **g-i**).

1193

1194

1195 **Extended Data Figure 7. Analysis of astrocyte development in the *Sox9-cKO* and**
1196 ***Nfia-cKO* mouse lines.**

1197 **a.** Analysis of NFIA expression in Aldh1l1-GFP astrocytes from the *Nfia-cKO* and
1198 *control* at P7 in the cortex, hippocampus, and olfactory bulb; quantification of knockout

bioRxiv preprint doi: https://doi.org/10.1101/2023.03.14.532493; this version posted March 15, 2023. The copyright holder for this preprint (which was not certified by peer review) is the author/funder, who has granted bioRxiv a license to display the preprint in perpetuity. It is made available under aCC-BY-NC-ND 4.0 International license.

1199 efficiency was derived from 3 pairs of animals (two-way ANOVA, *****P*<0.0001). **b.**
1200 Analysis of SOX9 expression in Aldh1l1-GFP astrocytes from the *Sox9-cKO* and *control*
1201 at P7 in the cortex, hippocampus, and olfactory bulb; quantification of knockout
1202 efficiency was derived from 3 pairs of animals (two-way ANOVA, *****P*<0.0001). **c.**
1203 Analysis of NFIA expression in Aldh1l1-GFP astrocytes from the *Nfia-cKO* and *control*
1204 at P28 in the cortex, hippocampus, cerebellum, and olfactory bulb; quantification of
1205 knockout efficiency was derived from 3 pairs of animals (two-way ANOVA,
1206 *****P*<0.0001). **d.** Analysis of SOX9 expression in Aldh1l1-GFP astrocytes from the
1207 *Sox9-cKO* and *control* at P28 in the cortex, hippocampus, cerebellum, and olfactory
1208 bulb; quantification of knockout efficiency was derived from 3 pairs of animals (two-way
1209 ANOVA, *****P*<0.0001, **P* = 0.0205). **e-f.** Two-photon, slice imaging of spontaneous
1210 GCaMP6s activity in *control* and *Nfia-cKO* astrocytes from the cortex at P28 (e) or
1211 *control* and *Sox9-cKO* astrocytes from the olfactory bulb at P28 (f); quantification is
1212 derived from 3 pairs of animals (two-tailed Mann-Whitney test). **g**. AAV-based
1213 overexpression of NFIA in the developing cortex, analysis of *Gabbr1* expression at P28
1214 via RNAscope; *n* = 3 pairs of animals (19, 18 cells; LME model, **P* = 0.023, ****P* =
1215 0.00034). **h**. AAV-based overexpression of SOX9 in the developing olfactory bulb,
1216 analysis of *Gabbr1* expression at P28 via RNAscope; *n* = 3 pairs of animals (20,25
1217 cells). Scale bars, 50 μm (**a-d**), 10 μm (**e-f**), 20 μm (**g-h**). Data represent mean ± s.d. (**a-**
1218 **d**), mean ± s.e.m. (**e-f**), median, minimum value, maximum value and IQR (**g**-**h**).
1219
1220 **Extended Data Figure 8. Analysis of astrocyte morphogenesis in the *Sox9-cKO***
1221 **and *Nfia-cKO* mouse lines.**

bioRxiv preprint doi: https://doi.org/10.1101/2023.03.14.532493; this version posted March 15, 2023. The copyright holder for this preprint (which was not certified by peer review) is the author/funder, who has granted bioRxiv a license to display the preprint in perpetuity. It is made available under aCC-BY-NC-ND 4.0 International license.

1222 **a-b.** Imaging of Aldh1l1-GFP astrocytes from the hippocampus, brainstem, and
1223 cerebellum at P28 from the *Nfia-cKO* (a) or *Sox9-cKO* (b) and associated controls;
1224 quantification of morphological complexity via Scholl analysis was derived from $n = 3$
1225 pairs of animals (**a**, *Nfia control*: HC 64, BS 28, CB 47; *Nfia cKO*: HC 65, BS 43, CB 55
1226 cells; GLME model with Sidak's multiple comparisons test, $^{**}P = 0.0015$; **b**, *Sox9*
1227 *control*: HC 32, BS 36, CB 32; *Sox9 cKO*: HC 24, BS 24, CB 37; GLME model with
1228 Sidak's multiple comparisons test). **c-d.** Quantification of astrocytic branch number and
1229 process length from *Nfia-cKO* (c) or *Sox9-cKO* (d) across cortex, olfactory bulb,
1230 hippocampus, brainstem, and cerebellum; derived from $n = 3$ pairs of animals (**c**, *Nfia*
1231 *control*: OB 59, CX 43, HC 54, BS 27, CB 48; *Nfia cKO*: OB 50, CX 56, HC 59, BS 38,
1232 CB 54 cells; two-way ANOVA, $^{**}P = 0.0054$, $^{****}P < 0.0001$; **d**, *Sox9 control*: OB 29, CX
1233 31, HC 32, BS 37, CB 33; *Sox9 cKO*: OB 40, CX 27, HC 33, BS 21, CB 39; two-way
1234 ANOVA, $^{**}P = 0.0025$, $^{****}P < 0.0001$, $^{***}P = 0.0002$). **e-f.** Pulse-chase EdU-labeling
1235 and antibody staining at P28 from the cortex of *Nfia-cKO* (e) and olfactory bulb of Sox9-
1236 cKO (f); quantification is derived from 3 pairs of animals (two-tailed Mann-Whitney test).
1237 **g-h.** Quantification of the number of Aldh1l1-GFP astrocytes in the cortex of the *Nfia-*
1238 *cKO* (g) or olfactory bulb from *Sox9-cKO* and associated controls; quantification is
1239 derived from 3 pairs of animals (two-tailed Mann-Whitney test). Scale bars, 30 μm (**a-b**),
1240 50 μm (**e-h**). Data represent mean ± s.d. (**a-h**).
1241
1242 **Extended Data Figure 9. Electrophysiological and behavioral analysis of the *Nfia-***
1243 ***cKO* mouse line.**

bioRxiv preprint doi: https://doi.org/10.1101/2023.03.14.532493; this version posted March 15, 2023. The copyright holder for this preprint (which was not certified by peer review) is the author/funder, who has granted bioRxiv a license to display the preprint in perpetuity. It is made available under aCC-BY-NC-ND 4.0 International license.

1244 **a.** Schematic of synaptic markers and cortical layers. **b-c.** Antibody staining for makers
1245 of excitatory synapses Vglut1/PSD95 (b) and Vglut2/PSD95 (c) in layer I of the cortex
1246 from NFIA-cKO or control mice at P28, quantification is derived from 3 pairs of animals
1247 (GLME model). **d.** Antibody staining for markers of inhibitory synapses VGAT/Gephyrin
1248 at P28; quantification is derived from 3 pairs of animals (GLME model). **e-f.**
1249 Representative traces of spontaneous EPSCs and IPSCs from excitatory (e) and
1250 inhibitory (f) neurons from cortex of *Nfia-cKO* and *controls*. Associated cumulative and
1251 bar plots demonstrate quantification of amplitude and frequency of sEPSC and sIPSC
1252 from 3 pairs of animals (**e**, Kolmogorov-Smirnov test, **** $P < 0.0001$, *$P = 0.0181$, two-
1253 tailed Mann-Whitney test; f, Kolmogorov-Smirnov test, **$P = 0.0026$, **** $P < 0.0001$,
1254 two-tailed Mann-Whitney test, *$P = 0.0149$). **g-h**. 3-chamber social interaction and
1255 prepulse inhibition behavioral studies on *Nfia-cKO* and *control* mice from 11-13 animals
1256 in each group (**g**, $n = 13$ pairs of animals, two-way ANOVA, ***$P = 0.0002$; **h**, $n = 13$, 11
1257 animals, two-tailed Mann-Whitney test, **$P = 0.0050$). **i-j**. Representative traces of
1258 action potential in layer II/III neurons upon varying injected current in *Nfia-cKO* and
1259 *control*. Summary data of action potential firing, resting membrane potential, and
1260 threshold from excitatory neurons (i) and inhibitory neurons (j); quantification is derived
1261 from at least 3 pairs of animals (two-way ANOVA and two-tailed Mann-Whitney test). **k-**
1262 **p.** Summary of behavioral tests from NFIA-cKO and control, including open field; $n = 13$,
1263 11 animals (k), elevated plus maze; $n = 10$ animals (l), rotarod; $n = 5$, 8 animals (m),
1264 parallel footfall; $n = 13$, 11 animals (n), contextual fear conditioning; $n = 12$, 10 animals
1265 (o), and cued fear conditioning; $n = 12$, 10 animals (p) (two-tailed Mann-Whitney test, *P

bioRxiv preprint doi: https://doi.org/10.1101/2023.03.14.532493; this version posted March 15, 2023. The copyright holder for this preprint (which was not certified by peer review) is the author/funder, who has granted bioRxiv a license to display the preprint in perpetuity. It is made available under aCC-BY-NC-ND 4.0 International license.

1266 = 0.0265, 0.0136). Scale bars, 3 μm (**b-d**). Data represent mean ± s.d. (**b-d**, **g**, **o-p**),
1267 mean ± s.e.m. (**e-f**, **h-n**)
1268

1269 **Extended Data Figure 10. Analysis of cortical neurons in the *Nfia-cKO* mouse line.**

1270 **a.** Antibody staining for BRN2 (Layers II/II), CTIP2 (Layers V), and FOXP2 (Layers VI)
1271 layer-specific neuronal markers in the P7 cortex from *Nfia-cKO* and control;
1272 quantification is derived from n = 3 pairs of animals (6 images, GLME model). **b.**
1273 Quantification of EDNRB expression in virally labeled astrocytes from the P28 cortex of
1274 mice where it has been knocked out using guideRNAs in the *ROSA-LSL-Cas9-EGFP*
1275 mouse line; quantification is derived from n = 3 pairs of animals (37, 38 cells; LME
1276 model, **P = 0.0068). **c**. Quantification of LHX2 expression in virally labeled astrocytes
1277 from the P28 cortex of mice where it has been knocked out using guideRNAs in the
1278 *ROSA-LSL-Cas9-EGFP* mouse line; quantification is derived from n = 3 pairs of animals
1279 (37, 39 cells; GLME model, ***P = 0.00099). **d-e.** Western blots before cropped, arrow
1280 heads label the proteins of interest. **f-g.** Imaging of virally labeled astrocytes from the
1281 P28 cortex of *Ednrb-cKO* or *Lhx2-cKO* mice where *Ednrb* or *Lhx2* has been knocked
1282 out using guideRNAs in the ROSA-LSL-Cas9-EGFP mouse line; quantification of
1283 morphological complexity via Scholl analysis was derived from n = 3 animals (**f**, *Ednrb-*
1284 *cKO*: 22 mcherry$^-$Cas9-EGFP$^+$ cells, 49 mcherry$^+$Cas9-EGFP$^+$ cells; GLME model with
1285 Sidak's multiple comparisons test, *P = 0.0307; GLME model, P = 0.06, **P = 0.008; **g**,
1286 *Lhx2-cKO*: 13 mcherry$^-$Cas9-EGFP$^+$ cells, 40 mcherry$^+$Cas9-EGFP$^+$ cells; GLME model
1287 with Sidak's multiple comparisons test, **P = 0.0037; GLME model, **P = 0.006, 0.003).

bioRxiv preprint doi: https://doi.org/10.1101/2023.03.14.532493; this version posted March 15, 2023. The copyright holder for this preprint (which was not certified by peer review) is the author/funder, who has granted bioRxiv a license to display the preprint in perpetuity. It is made available under aCC-BY-NC-ND 4.0 International license.

1288 Scale bars, 100 μm (**a**). Data represent mean ± s.d. (**a**, **f-g** left), median, minimum value,

1289 maximum value and IQR (**b-c**, **f-g** right).

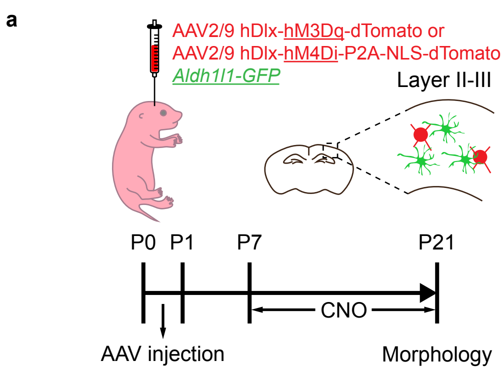
a
AAV2/9 hDlx-hM3Dq-dTomato or
AAV2/9 hDlx-hM4Di-P2A-NLS-dTomato
Aldh1l1-GFP
Layer II-III
P0
P1
P7
P21
CNO
AAV injection
Morphology

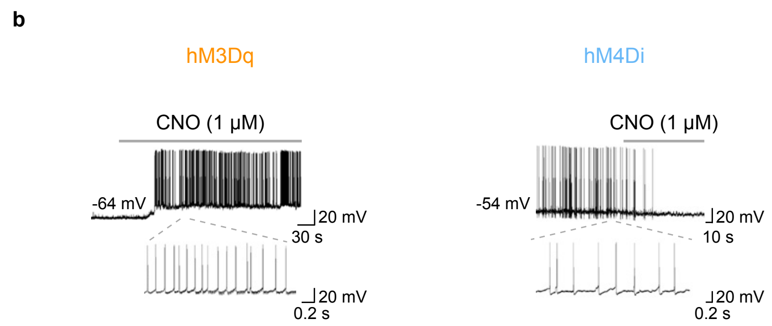
b
hM3Dq
hM4Di
CNO (1 μM)
CNO (1 μM)
-64 mV
-54 mV
20 mV
30 s
20 mV
10 s
20 mV
0.2 s
20 mV
0.2 s

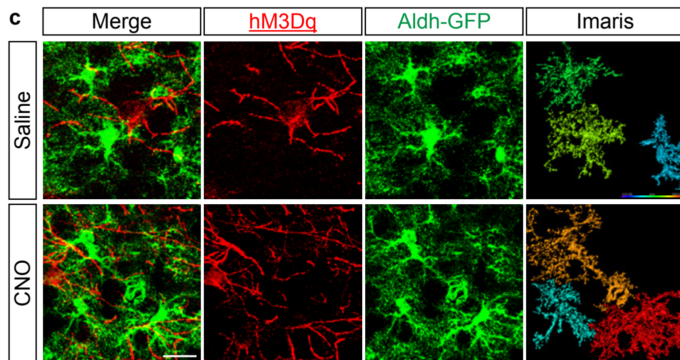
c
Merge
hM3Dq
Aldh-GFP
Imaris
Saline
CNO

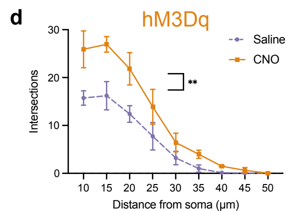
d
hM3Dq
Saline
CNO
Intersections
Distance from soma (μm)
**

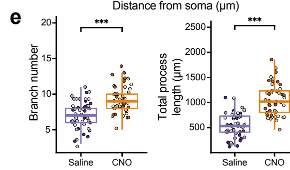
e
Branch number
Total process length (μm)
Saline
CNO
***
***

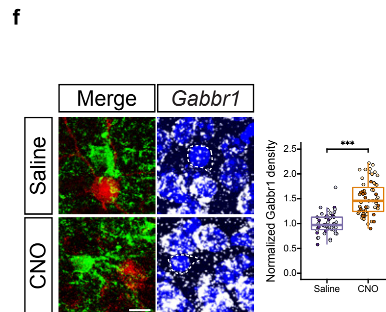
f
Merge
Gabbr1
Saline
CNO
Normalized Gabbr1 density
***
Saline
CNO

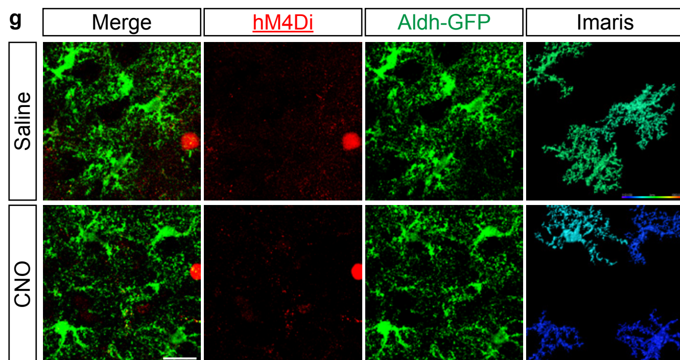
g
Merge
hM4Di
Aldh-GFP
Imaris
Saline
CNO

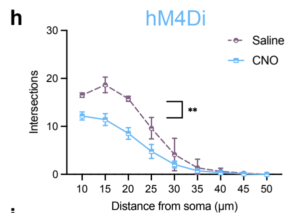
h
hM4Di
Saline
CNO
Intersections
Distance from soma (μm)
**

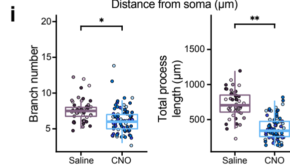
i
Branch number
Total process length (μm)
Saline
CNO
*
**

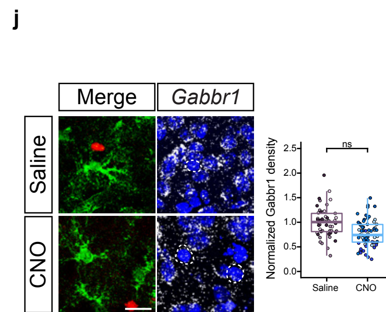
j
Merge
Gabbr1
Saline
CNO
Normalized Gabbr1 density
ns
Saline
CNO

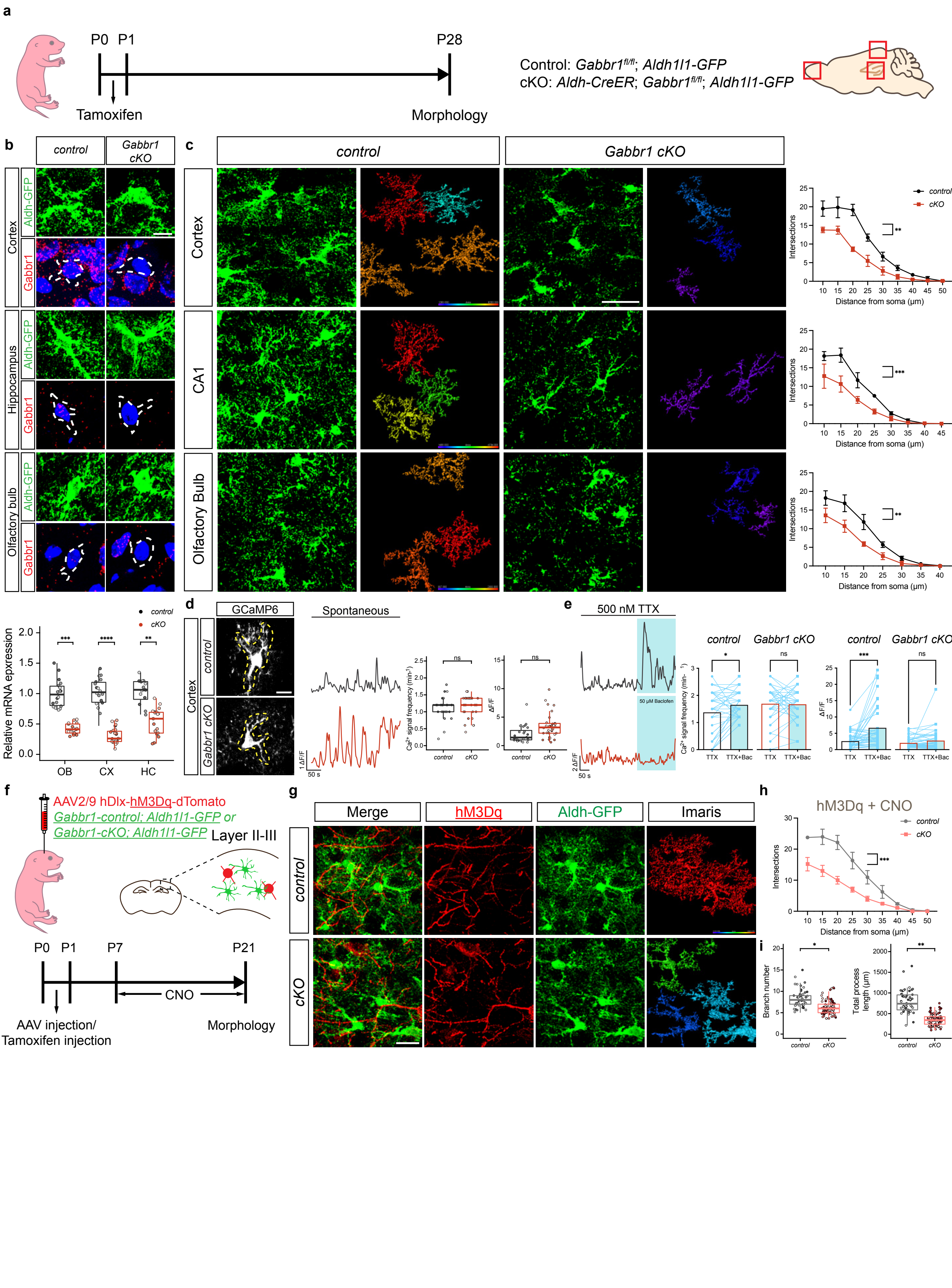

a
P0
P1
P28
Tamoxifen
Morphology
Control: Gabbr1fl/fl; Aldh1l1-GFP
cKO: Aldh-CreER; Gabbr1fl/fl; Aldh1l1-GFP
b
control
Gabbr1 cKO
Cortex
Hippocampus
Olfactory bulb
Aldh-GFP
Gabbr1
c
control
Gabbr1 cKO
Cortex
CA1
Olfactory Bulb
Intersections
Distance from soma (μm)
control
cKO
Relative mRNA epxression
OB
CX
HC
d
GCaMP6
Spontaneous
Gabbr1 cKO
Ca2+ signal frequency (min-1)
ΔF/F
ns
50 s
e
500 nM TTX
50 μM Baclofen
TTX
TTX+Bac
f
AAV2/9 hDlx-hM3Dq-dTomato
Gabbr1-control; Aldh1l1-GFP or
Gabbr1-cKO; Aldh1l1-GFP
Layer II-III
P0
P1
P7
P21
CNO
AAV injection/
Tamoxifen injection
Morphology
g
Merge
hM3Dq
Aldh-GFP
Imaris
h
hM3Dq + CNO
i
Branch number
Total process length (μm)

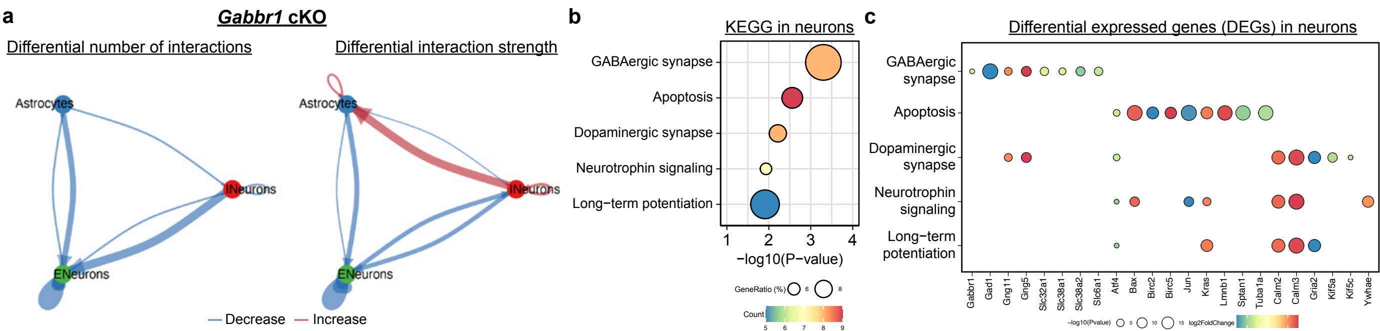

a
Gabbr1 cKO
Differential number of interactions
Differential interaction strength
Astrocytes
INeurons
ENeurons
Decrease
Increase
b
KEGG in neurons
GABAergic synapse
Apoptosis
Dopaminergic synapse
Neurotrophin signaling
Long−term potentiation
−log10(P−value)
GeneRatio (%)
Count
c
Differential expressed genes (DEGs) in neurons
GABAergic synapse
Apoptosis
Dopaminergic synapse
Neurotrophin signaling
Long−term potentiation
Gabbr1
Gad1
Gng11
Gng5
Slc32a1
Slc38a1
Slc38a2
Slc6a1
Atf4
Bax
Birc2
Birc5
Jun
Kras
Lmnb1
Sptan1
Tuba1a
Calm2
Calm3
Gria2
Kif5a
Kif5c
Ywhae

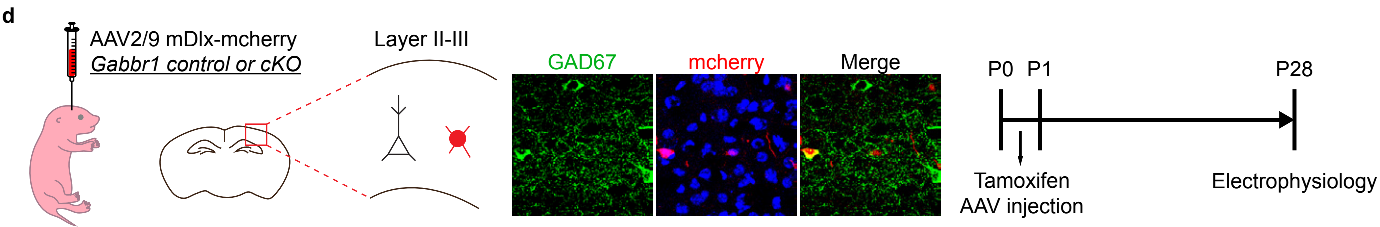

d
AAV2/9 mDlx-mcherry
Gabbr1 control or cKO
Layer II-III
GAD67
mcherry
Merge
P0
P1
P28
Tamoxifen
AAV injection
Electrophysiology

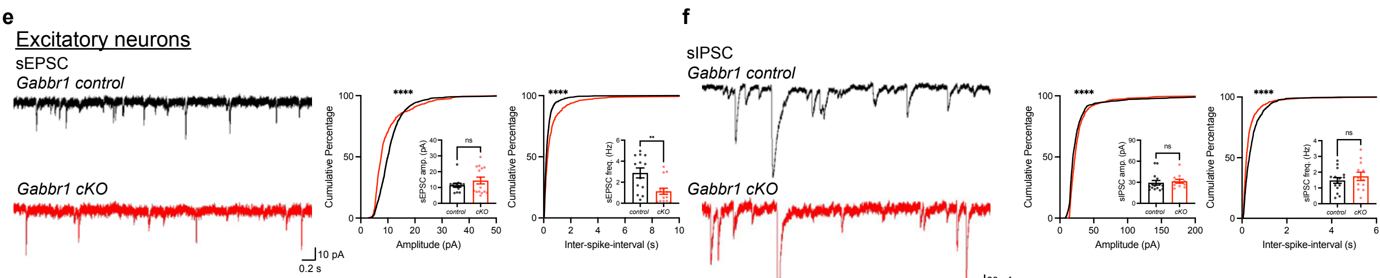

e
Excitatory neurons
sEPSC
Gabbr1 control
Gabbr1 cKO
10 pA
0.2 s
Cumulative Percentage
Amplitude (pA)
Inter-spike-interval (s)
f
sIPSC
Gabbr1 control
Gabbr1 cKO
20 pA
0.2 s

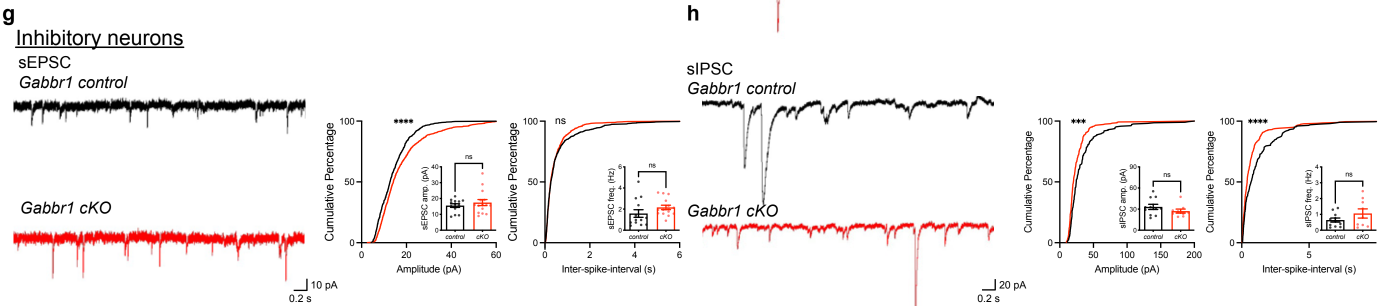

g
Inhibitory neurons
sEPSC
Gabbr1 control
Gabbr1 cKO
10 pA
0.2 s
Cumulative Percentage
Amplitude (pA)
Inter-spike-interval (s)
h
sIPSC
Gabbr1 control
Gabbr1 cKO
20 pA
0.2 s

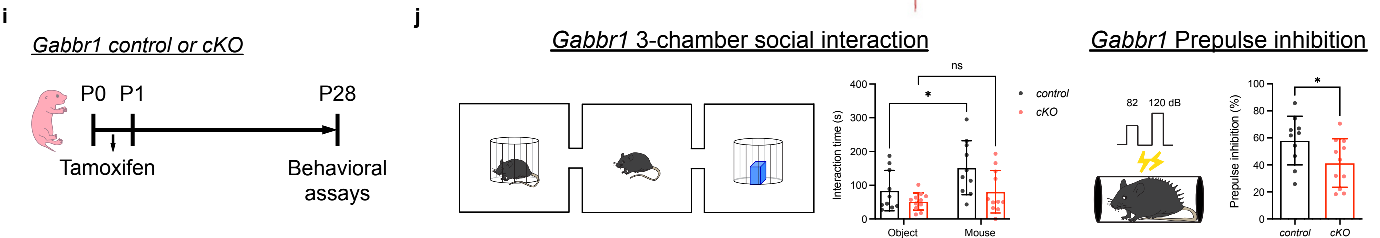

i
Gabbr1 control or cKO
P0
P1
P28
Tamoxifen
Behavioral assays
j
Gabbr1 3-chamber social interaction
Interaction time (s)
Object
Mouse
control
cKO
Gabbr1 Prepulse inhibition
82
120 dB
Prepulse inhibition (%)
control
cKO

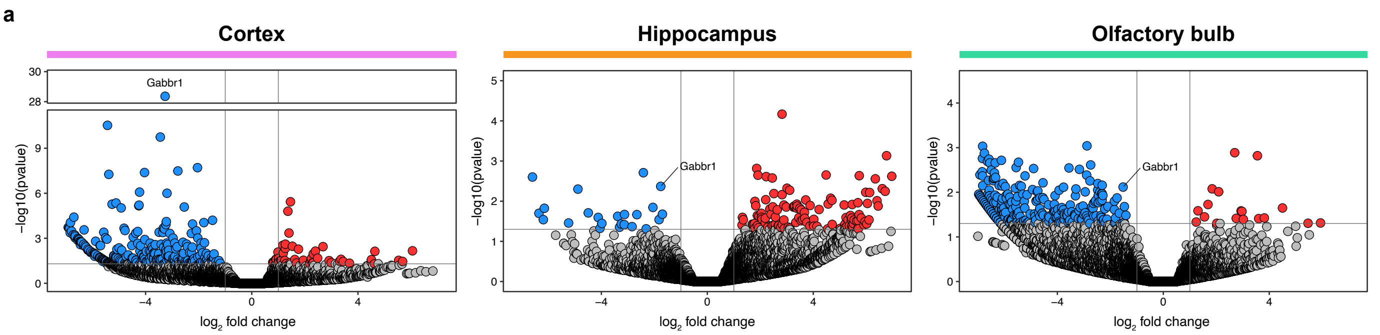

a
Cortex
Hippocampus
Olfactory bulb
Gabbr1
−log10(pvalue)
log2 fold change

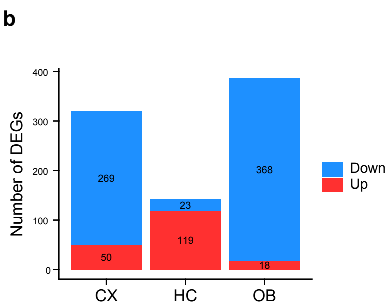

b
Number of DEGs
Down
Up
269
50
23
119
368
18
CX
HC
OB

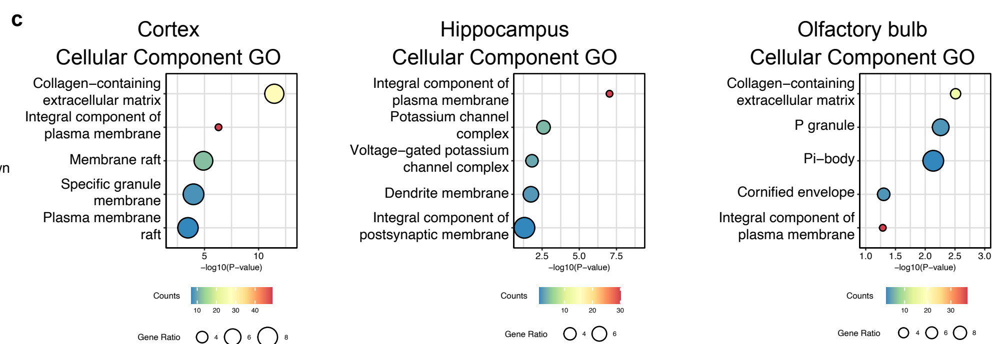

c
Cortex
Cellular Component GO
Collagen−containing extracellular matrix
Integral component of plasma membrane
Membrane raft
Specific granule membrane
Plasma membrane raft
Hippocampus
Cellular Component GO
Integral component of plasma membrane
Potassium channel complex
Voltage−gated potassium channel complex
Dendrite membrane
Integral component of postsynaptic membrane
Olfactory bulb
Cellular Component GO
Collagen−containing extracellular matrix
P granule
Pi−body
Cornified envelope
Integral component of plasma membrane
−log10(P−value)
Counts
Gene Ratio

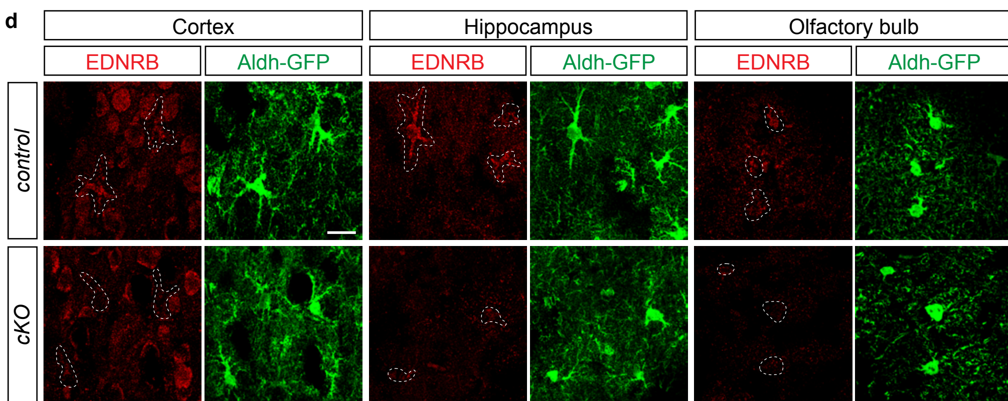

d
Cortex
Hippocampus
Olfactory bulb
EDNRB
Aldh-GFP
control
cKO

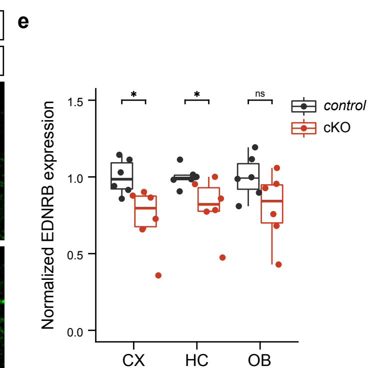

e
Normalized EDNRB expression
control
cKO
ns
CX
HC
OB

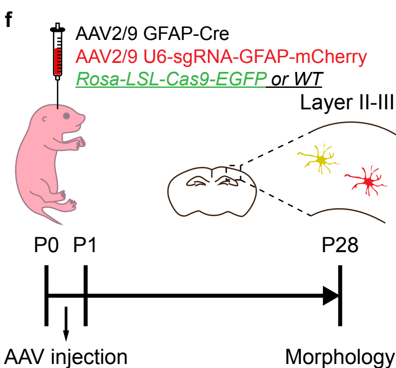

f
AAV2/9 GFAP-Cre
AAV2/9 U6-sgRNA-GFAP-mCherry
Rosa-LSL-Cas9-EGFP or WT
Layer II-III
P0
P1
P28
AAV injection
Morphology

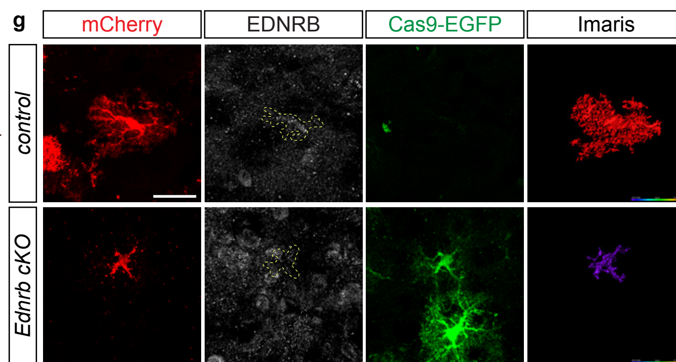

g
mCherry
EDNRB
Cas9-EGFP
Imaris
control
Ednrb cKO

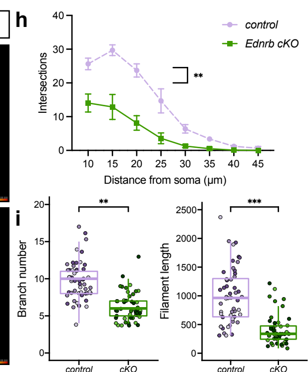

h
control
Ednrb cKO
Intersections
Distance from soma (μm)
i
Branch number
Filament length
control
cKO

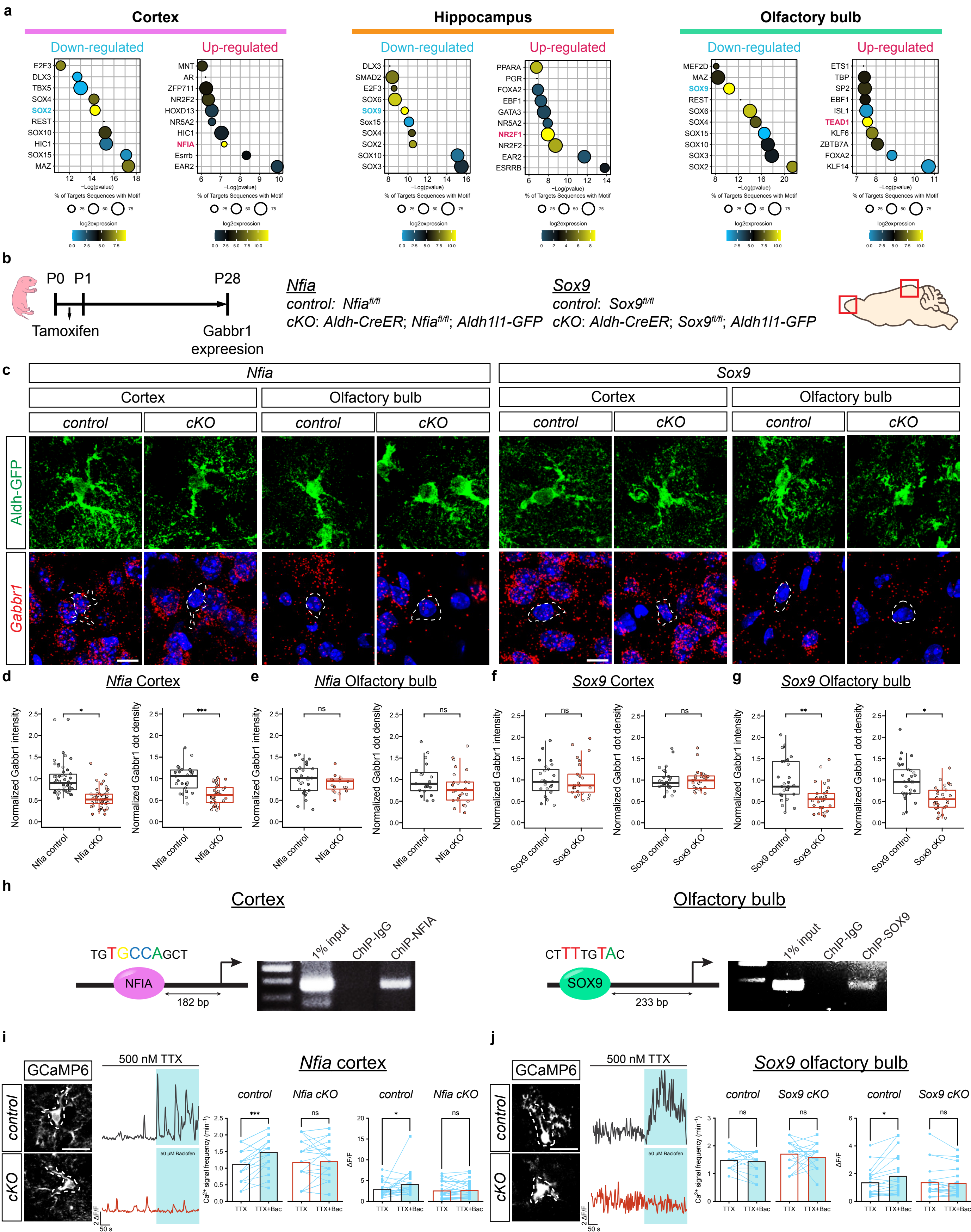

a
Cortex
Hippocampus
Olfactory bulb
Down-regulated
Up-regulated
−Log(pvalue)
% of Targets Sequences with Motif
log2expression
b
P0
P1
P28
Tamoxifen
Gabbr1 expression
Nfia
control: Nfia fl/fl
cKO: Aldh-CreER; Nfia fl/fl; Aldh1l1-GFP
Sox9
control: Sox9 fl/fl
cKO: Aldh-CreER; Sox9 fl/fl; Aldh1l1-GFP
c
Nfia
Sox9
Cortex
Olfactory bulb
control
cKO
Aldh-GFP
Gabbr1
d
Nfia Cortex
e
Nfia Olfactory bulb
f
Sox9 Cortex
g
Sox9 Olfactory bulb
Normalized Gabbr1 intensity
Normalized Gabbr1 dot density
Nfia control
Nfia cKO
Sox9 control
Sox9 cKO
h
Cortex
Olfactory bulb
TGTGCCAGCT
NFIA
182 bp
1% input
ChIP-IgG
ChIP-NFIA
CTTTTGTAC
SOX9
233 bp
ChIP-SOX9
i
GCaMP6
500 nM TTX
50 μM Baclofen
Nfia cortex
Nfia cKO
Ca2+ signal frequency (min−1)
ΔF/F
TTX
TTX+Bac
2 ΔF/F
50 s
j
Sox9 olfactory bulb
Sox9 cKO

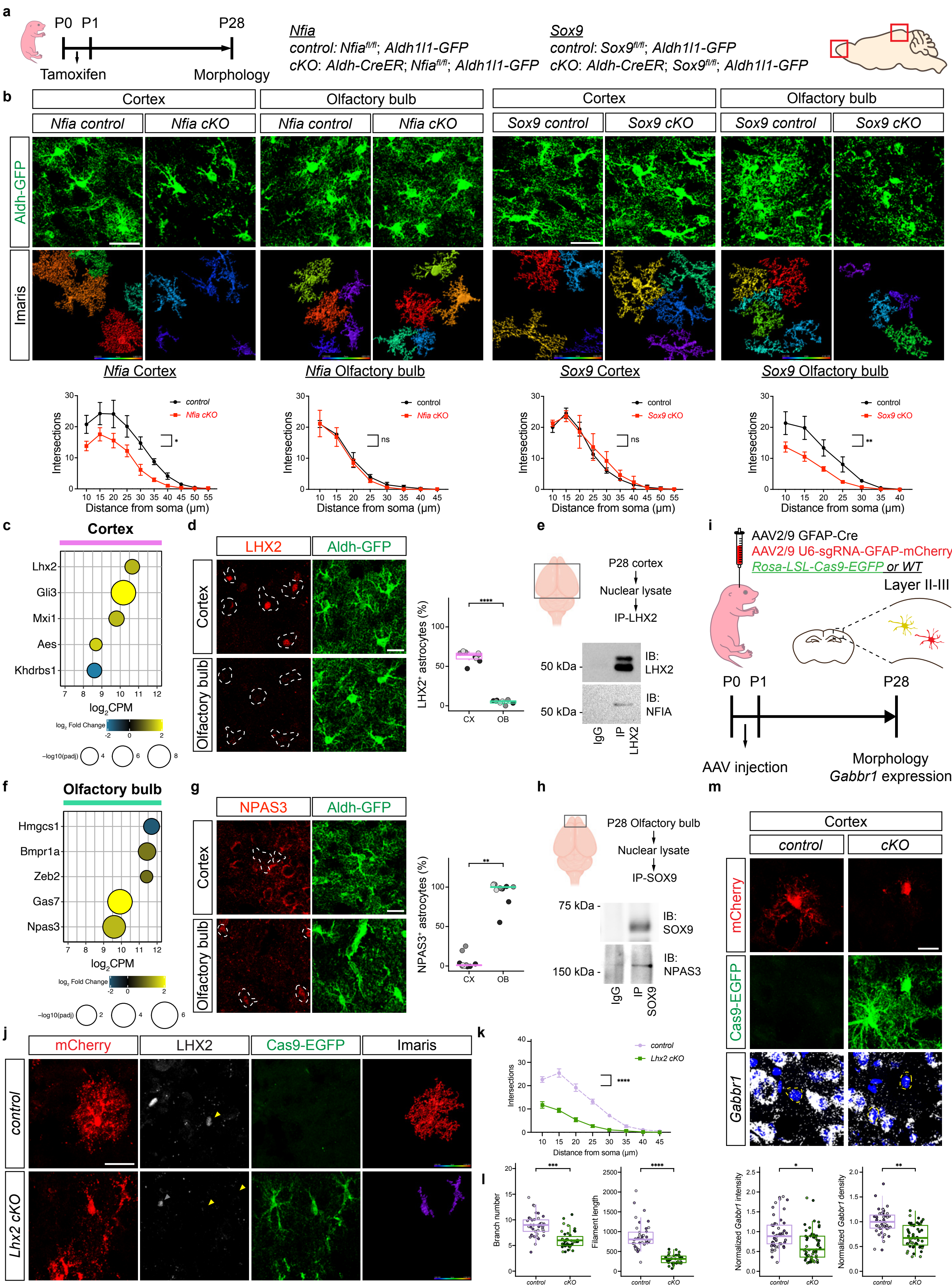
a
P0 P1 P28
Tamoxifen
Morphology
Nfia
control: Nfiafl/fl; Aldh1l1-GFP
cKO: Aldh-CreER; Nfiafl/fl; Aldh1l1-GFP
Sox9
control: Sox9fl/fl; Aldh1l1-GFP
cKO: Aldh-CreER; Sox9fl/fl; Aldh1l1-GFP
b
Cortex
Olfactory bulb
Nfia control
Nfia cKO
Sox9 control
Sox9 cKO
Aldh-GFP
Imaris
Nfia Cortex
Nfia Olfactory bulb
Sox9 Cortex
Sox9 Olfactory bulb
control
Nfia cKO
Sox9 cKO
Intersections
Distance from soma (μm)
ns
c
Cortex
Lhx2
Gli3
Mxi1
Aes
Khdrbs1
log2CPM
log2 Fold Change
−log10(padj)
d
LHX2
Aldh-GFP
Cortex
Olfactory bulb
LHX2+ astrocytes (%)
CX
OB
e
P28 cortex
Nuclear lysate
IP-LHX2
50 kDa
IB: LHX2
IB: NFIA
IgG
IP LHX2
i
AAV2/9 GFAP-Cre
AAV2/9 U6-sgRNA-GFAP-mCherry
Rosa-LSL-Cas9-EGFP or WT
Layer II-III
P0 P1 P28
AAV injection
Morphology
Gabbr1 expression
f
Olfactory bulb
Hmgcs1
Bmpr1a
Zeb2
Gas7
Npas3
g
NPAS3
Aldh-GFP
NPAS3+ astrocytes (%)
h
P28 Olfactory bulb
Nuclear lysate
IP-SOX9
75 kDa
150 kDa
IB: SOX9
IB: NPAS3
IP SOX9
m
Cortex
control
cKO
mCherry
Cas9-EGFP
Gabbr1
j
mCherry
LHX2
Cas9-EGFP
Imaris
control
Lhx2 cKO
k
control
Lhx2 cKO
Intersections
Distance from soma (μm)
l
Branch number
Filament length
control
cKO
Normalized Gabbr1 intensity
Normalized Gabbr1 density